

On the Frequency of Jupiter Analogs

Robert A. Wittenmyer¹, C.G. Tinney¹, Simon J. O’Toole², H.R.A. Jones³, R.P. Butler⁴,
B.D. Carter⁵, J. Bailey¹

rob@phys.unsw.edu.au

ABSTRACT

The Anglo-Australian Planet Search has now accumulated 12 years of radial-velocity data with long-term instrumental precision better than 3 m s^{-1} . In this paper, we expand on earlier simulation work, to probe the frequency of near-circular, long-period gas-giant planets residing at orbital distances of 3-6 AU – the so-called “Jupiter analogs.” We present the first comprehensive analysis of the frequency of these objects based on radial-velocity data. We find that 3.3% of stars in our sample host Jupiter analogs; detailed, star-by-star simulations show that no more than 37% of stars host a giant planet between 3–6 AU.

Subject headings: planetary systems – techniques: radial velocities

1. Introduction

Recent discoveries of ever lower-mass planets have received a great deal of publicity. Equally important, however, are discoveries of long-period planets. A long-standing question in astrophysics is “How common are planetary systems like our own Solar system?” The so-called “Jupiter analogs,” with orbital periods $P \gtrsim 10$ years and velocity amplitudes $K \sim 10 \text{ m s}^{-1}$, represent another means for probing the frequency of systems with architectures

¹Department of Astrophysics, School of Physics, University of NSW, 2052, Australia

²Anglo-Australian Observatory, PO Box 296, Epping, 1710, Australia

³Centre for Astrophysics Research, University of Hertfordshire, College Lane, Hatfield, Herts AL10 9AB, UK

⁴Department of Terrestrial Magnetism, Carnegie Institution of Washington, 5241 Broad Branch Road, NW, Washington, DC 20015-1305, USA

⁵Faculty of Sciences, University of Southern Queensland, Toowoomba, Queensland 4350, Australia

similar to our Solar system¹. Such planets are now within the reach of the longest-running radial-velocity planet-search programs. A critical part of addressing the key question of Solar system frequency is assessing the selection effects at work in the regime of long-period, Jovian planets.

Microlensing observations are beginning to be effective in detecting and constraining the population of Jupiter-like planets. The gravitational microlensing technique is well-suited to detecting planets which have not experienced significant inward migration, typically at separations $a > 3$ AU (cf. Fig. 9 from Sumi et al. 2010). The discovery of a Jupiter/Saturn analog by Gaudi et al. (2008) illustrates the power of the microlensing technique to detect planets which are currently beyond the reach (in both observation time and precision) of Doppler measurements. Gould et al. (2010) presented the first estimate of the frequency of planets beyond the snow line, based on a sample of 6 microlensing planet discoveries.

Previously published analyses of radial-velocity data sets have been able to place upper limits on substellar and planetary companions from radial-velocity surveys. Murdoch et al. (1993) determined detection limits for the Mt. John radial-velocity program by adding the program’s mean velocity error (65 m s^{-1}) to the signals of planets in circular orbits. Planetary signals were then recovered by the periodogram and F-test methods, and those planets for which 95% of phases were recovered with false-alarm probability (FAP) < 1% were considered detectable. They were able to exclude planets with $m \sin i > 10 M_{\text{Jup}}$ with periods less than 2000 days, and brown dwarf companions ($10\text{-}40 M_{\text{Jup}}$) with $P < 8.2$ years. Similarly, Cumming et al. (1999) computed detection limits from the Lick planet search data by 1) noting the highest peak z_{max} in the periodogram for each target, and 2) generating simulated data sets with sinusoidal (circular-orbit) signals and finding the velocity amplitude K for which 99% of signals had power exceeding z_{max} . They achieved a detection limit of 20 m s^{-1} for companions with $a \lesssim 5$ AU. The 12-year CFHT survey of Walker et al. (1995), with a velocity precision of 15 m s^{-1} , achieved detection limits approaching a Jupiter mass for planets in circular orbits and periods shorter than ~ 10 yr. Wittenmyer et al. (2006) combined the data of Walker et al. (1995) with data from the McDonald Observatory planet search to achieve a baseline of more than 20 years for a sample of 31 bright solar-type stars. Those authors estimated a 99% detection limit of $2.0 \pm 1.1 M_{\text{Jup}}$ for planets in Jupiter-like orbits ($e = 0.0$, $a = 5.2$ AU). Recently, Cumming et al. (2008) presented a detailed analysis of 8 years of Keck Planet Search data (585 stars with $N > 10$ measurements), resulting in a typical detection limit of 10 m s^{-1} for periods less than the duration of the observations. From those data, Cumming et al. (2008) estimated a giant planet ($0.3\text{-}10 M_{\text{Jup}}$) frequency

¹For Jupiter, $P = 11.86\text{yr}$ and $K = 12.5 \text{ m s}^{-1}$.

of 10.5% for orbital periods less than 2000 days.

The Anglo-Australian Planet Search (AAPS) has been in operation since 1998 January, and currently monitors 250 stars. The AAPS has achieved a long-term radial-velocity precision of 3 m s^{-1} or better since its inception, which is enabling the detection of long-period giant planets. These planets have typical velocity amplitudes $K \lesssim 15 \text{ m s}^{-1}$, and their detection requires superb long-term velocity stability. Some notable recent AAPS detections of such planets include HD 134987c (Jones et al. 2010: $P = 13.7 \text{ yr}$, $M \sin i = 0.82 M_{\text{Jup}}$, $K = 9 \text{ m s}^{-1}$) and GJ 832b (Bailey et al. 2009: $P = 9.4 \text{ yr}$, $M \sin i = 0.64 M_{\text{Jup}}$, $K = 15 \text{ m s}^{-1}$). The long-term precision of the AAT/UCLES system has enabled the AAPS to be relatively efficient at detecting long-period planets. Of the planets discovered by the AAPS, $37 \pm 11\%$ have periods longer than 1000 days. For comparison, this figure is $29 \pm 5\%$ for the Lick & Keck program, $18 \pm 4\%$ for HARPS+CORALIE+ELODIE, and $14 \pm 6\%$ for all other planet-search teams. These figures are obtained by counting the number of planets with $P > 1000$ days discovered by each group, then dividing by the total number of planets discovered by that group.² As the AAPS now spans 12 years, it is important to make quantitative estimates of the population of detectable Jupiter analogs in our sample and in the Solar neighbourhood.

Here we define a “Jupiter analog” as a planet with a small eccentricity ($e < 0.2$) and a long period ($P \gtrsim 8 \text{ yr}$). That is, a giant planet which plays a dynamical role similar to that of our own Jupiter, with a period long enough to imply *in situ* formation, and an eccentricity low enough to suggest a benign dynamical history. In this paper, we present detection limits for Jupiter analogs from the 12-year AAPS database. Section 2 briefly describes the observational data, and Section 3 discusses the techniques used to calculate detection limits. In Section 4, we present the results, and in Section 5 we discuss the results in the broader context of the population of long-period planets.

2. Observations

AAPS Doppler measurements are made with the UCLES echelle spectrograph (Diego et al. 1991). An iodine absorption cell provides wavelength calibration from 5000 to 6200 Å. The spectrograph point-spread function and wavelength calibration are derived from the iodine absorption lines embedded on every pixel of the spectrum by the cell (Valenti et al. 1995; Butler et al. 1996). The result is a precision Doppler velocity estimate for each epoch, along with an internal uncertainty estimate, which includes the effects of photon-counting uncertainties, residual errors in the spectrograph PSF model, and variation in the underlying

²Planet data obtained from the Exoplanet Data Explorer at exoplanets.org

spectrum between the iodine-free template, and epoch spectra observed through the iodine cell. All velocities are measured relative to the arbitrary zero-point defined by the template observation.

The AAPS target list contains 254 stars, of which 180 have been observed for more than 8 years. Since the aim of this work is to place meaningful limits on Jupiter analogs, here we only consider those stars which have more than 8 years of data ($N = 180$). We further restrict the sample to those stars which have been observed more than 30 times ($N = 123$). This is because the reliability of the FAP calculation is strongly dependent on the number of data points.

Table 1 summarises the data characteristics for these 123 stars. For those stars with long-term trends indicating a distant stellar companion, a linear or quadratic fit was removed from the data before subjecting them to the detection-limit procedure. For stars known to host a substellar companion, we did a fit for and removed that orbit and then performed the detection-limit computations on the residuals.

3. Computational Methods

A set of simulations such as these is only as meaningful as the input assumptions and parameters. In this section, we give a detailed discussion of our choices for these simulations.

3.1. The Detection Limit Algorithm

The detection limits were computed using the method of Wittenmyer et al. (2006). In brief, we add a Keplerian signal to the existing velocity data, then attempt to recover that signal using a Lomb-Scargle periodogram. The mass of the simulated planet is increased until 99% of the injected signals are recovered with $\text{FAP} < 0.1\%$. For a given mass (or equivalently, a given velocity amplitude) at a given orbital period, we use a grid of 30 values of periastron passage T_0 and, for eccentric orbits, 18 values of the periastron argument ω spaced evenly every 20 degrees. This makes a total of 30 possible orbital configurations for simulated planets with $e = 0.0$, and 540 configurations for those with eccentric orbits. We simulated planets over 100 orbital periods ranging from 1000 to 5000 days, evenly spaced in the logarithm of the period. For a simulated planet with amplitude K to be considered detectable at the 99% level, we must recover 99% of configurations (30/30 for circular orbits, 535/540 for eccentric orbits). A successful recovery occurs when the injected period is the highest peak in the periodogram, has a FAP less than 0.1%, and the recovered period is

within a specified tolerance of the injected period; Section 3.2 gives additional details on the selection of this tolerance. In addition to the 99% recovery level, we performed these simulations at recovery levels of 90, 70, and 50%, to maintain consistency with our previous simulation work (O’Toole et al. 2009c; Wittenmyer et al. 2010). Hereafter, we refer to each set of simulations by its eccentricity and recovery rate: for example, the set where $e = 0.1$ at 90% recovery is referred to as “e01r90.” The result of these simulations is, for each star, a plot of the K amplitude (or planet mass) recovered in (99%, 90%, 70%, 50%) of trials at each orbital period between 1000 and 5000 days.

Figure 1, which shows the distribution of FAP for all simulated signals which were considered successfully recovered in the e00r99 trials, demonstrates our reasoning in choosing a cutoff criterion of $\text{FAP} < 0.1\%$. Summed over all 123 stars, the histogram includes results from 362368 simulated signals. Though the cutoff criterion was $\text{FAP} < 0.1\%$ (0.001), it is evident that the vast majority of recovered signals achieved FAP values that are far more significant. The distribution has two peaks, at 10^{-4} ($N \sim 12000$) and $< 10^{-9}$ ($N = 66784$). The latter of these is an artifact, simply representing the integration over a long tail of $\text{FAP} < 10^{-9}$. If most trials resulted in $\text{FAP} > 10^{-3}$, the cutoff we have imposed would bias the derived detection limits. We would see such an effect in Figure 1 as a pile-up at the least significant bin ($\text{FAP} = 10^{-3}$). That the highest peaks in Figure 1 lie at FAP levels at least an order of magnitude more significant than the imposed cutoff indicates that our choice of cutoff has not biased the results.

In order to focus on potential Jupiter analogs, we only consider simulated planets with $e = 0.0, 0.1, \text{ and } 0.2$, in keeping with the $e < 0.2$ definition of “Jupiter analog” described in Section 1. These three values of e provide sufficient sampling of the relevant eccentricity range because, for long-period planets ($P > 1000$ days), the orbital eccentricity is typically determined only to an accuracy of 0.02-0.04. Figure 2 shows a histogram of the uncertainty in eccentricity (σ_e) for the 74 published planets with $P > 1000$ days. The peak of the distribution lies at $\sigma_e \sim 0.02\text{-}0.04$, with a median value of 0.05. We also note that published estimates of σ_e are often underestimated due to correlations between the Keplerian orbital parameters and the non-Gaussianity of their distributions (Ford 2005; O’Toole et al. 2009a). In particular, O’Toole et al. (2009a) found that the 99% confidence interval for eccentricity can be 10-50 times larger than the traditional uncertainty estimates derived from the covariance matrix in a least-squares Keplerian fit. This is particularly important when the signal of the planet (defined in O’Toole et al. 2009a as K/σ_K) is smaller than about 3. For these reasons, we have chosen a coarse grid of eccentricities for these simulations. A finer interval would vastly increase the computing time required without adding meaningful information.

3.2. False Positives and False Negatives

All previous implementations of this detection-limit algorithm (Wittenmyer et al. 2006, 2007, 2009, 2010) have used the criterion that the recovered period be within 5% of the input period of the simulated planet. The reason for this seemingly arbitrary criterion is that in the Lomb-Scargle periodogram, spurious peaks can arise due to the sampling of the data. Most common in radial-velocity data are the 1-year and 1-month aliases, the former due to targets becoming unobservable as they pass behind the Sun, and the latter due to telescope scheduling constraints which usually restrict planet-search observations to bright lunations. Harmonics of the injected periodicities (e.g. $P/2, 2 \times P$, etc.) also often produce significant periodogram peaks. Imposing the “correct-period” criterion reduces the effect of these features and thus minimises incorrect detections (false positives). For simulations such as these, involving a vast number of attempted planetary detections and using automated detection criteria, it is critical to understand and to minimise (or ideally, to eliminate) false positives. O’Toole et al. (2009a) presented a detailed discussion of the problem of false positives in simulations of planet-search data.

A potential pitfall in establishing detection criteria to minimise false positives is that, if those criteria are too stringent, false *negatives* become important. False negatives (i.e. incorrect rejections) are substantially more difficult to quantify, and hence are fiendishly difficult to control. In practice, because scientists rightfully consider incorrect detections to be a far more serious problem, much more effort is spent in eliminating false positives than false negatives. In the detection-limit algorithm described above, we seek to eliminate false positives by the imposition of the “correct-period” criterion. The FAP criterion alone (FAP < 0.001) eliminates some incorrect detections, but since the FAP calculation is dependent on the number of data points, even alias periodicities achieve high significance for larger data sets ($N \gtrsim 50$). We performed some tests with AAPS data (which have $N > 100$ for many targets), removing the correct-period criterion and relying on only the FAP criterion to eliminate false detections. Figure 3 shows the effect of different settings for the FAP criterion in this test. As expected, requiring a more significant periodogram recovery (i.e. a lower FAP cutoff) reduces the false-positive rate. However, there are two important consequences: 1) The false-positive rate remains at a nontrivial level even for extremely stringent FAP levels, and 2) When the FAP cutoff is set to such low levels, the detection-limit result is dominated by false negatives: nearly all of the injected trial signals are rejected, and no meaningful detection limit is obtained.

These tests demonstrated that a correct-period constraint is necessary to obtain useful detection limits and to control the false positive rate. The next question is then: How close to the input period does the recovered period need to be, to be considered a success-

ful detection? Too loose a constraint would degrade the scientific value of the detection limits obtained from this method, whereas too stringent a constraint results in the automated rejection of signals which a rational human investigator would consider sufficiently close (e.g. $P=3.05$ versus 3.04 days). The core question is: “What would a human do?” One way to approach this problem is to determine what other humans have already done. That is, what is the fractional uncertainty in orbital period at which authors have decided to publish a planet detection? Radial-velocity planet search teams generally prefer to wait until a complete orbital cycle has been observed before publishing a planet discovery. One expects the uncertainty in the fitted period (σ_P) to drop as more orbital cycles are observed. We performed an exhaustive literature search, locating the original discovery paper for every radial-velocity planet, and tabulating the period (P), period uncertainty (σ_P), and the total time-span of the observations (ΔT). In this search, we included only those planets: 1) which were originally detected by the radial-velocity method, and 2) where a refereed paper is available indicating the above-mentioned quantities. The reason for excluding planets discovered by transits is that the transit is a special circumstance which enables the orbital period to be determined to extremely high precision. That would skew the relation between σ_P/P and ΔT , which we seek to apply to the radial-velocity database of the Anglo-Australian Planet Search (which includes no transiting planets). The results of this search are shown in Figure 4. One readily evident feature is that no planets have been published with less than 0.7 cycles of data (vertical dashed line in the figure). Of the 290 planets, only 24 (8.3%) were published with less than one orbital cycle of data. The outlier with an unusually large fractional error in period ($\sigma_P/P=17.2\%$) is HD 149143 (Fischer et al. 2006). That planet was first published with only 17 observations, which may account for the large uncertainty in its 4-day period.

We wish to derive a relation between the data span ΔT (equivalently, the number of cycles), and the period error σ_P/P ; however, the number statistics of the known planets remain poor. Hence, we performed some additional simulations to fill out the ΔT - σ_P/P plane. For each of 210 stars in the AAPS database, we created 2000 simulated radial-velocity datasets. Each simulated dataset used the observation times and velocity uncertainties of the original observed data. The simulated planets had periods ranging from 5 to 5000 days (in a grid with a uniform spacing of 10 days), velocity amplitudes between 20-50 m s^{-1} , and eccentricities randomly drawn from the range 0.0 : 0.5. Noise (jitter) drawn from a Gaussian distribution with a width $\sigma = 5 \text{ m s}^{-1}$ was also added to each simulated velocity measurement. We then fit each dataset with a Keplerian model using GaussFit (Jefferys et al. 1987) and recorded the fitted period and its uncertainty. Since the maximum period used sometimes significantly exceeded the length of the available data for certain of the targets in the AAPS database, those fits often produced unphysical results, and were discarded.

Consistent with the characteristics of published planets described above, we also discarded all fits where less than 0.7 cycles of data were present. Of the 420000 simulations, 357681 remained after these cuts, and the results are plotted in Figure 5. We can now use these results to make an informed choice for the correct-period constraint. Since the injected trial period is assumed not to be known *a priori*, it is logical to choose the value of σ_P/P which includes 99% of the planets simulated in this section. This results in $\sigma_P/P = 27.7\%$, which is the value used for the correct-period constraint in all detection-limit simulations here.

Finally, we show in Figure 6 examples of a rejected and an accepted recovery using the methods described in this section. An input data file (HD 209653) was chosen at random for this demonstration. The left panel shows the periodogram resulting from an injected signal with $P = 1000$ days, $K = 1\text{ms}^{-1}$, and $e = 0.0$. As expected with such a weak signal, there is no compelling evidence for it in the periodogram; the highest peaks occur at 9.7 and 365 days, the latter an artefact of the window function (lower panels). The FAP of the 9.7-day peak was 0.018, much less significant than the cutoff of 0.001. The right panel of Figure 6 shows the periodogram resulting from the same dataset with an injected signal having $P = 1000$ days, $K = 10\text{ms}^{-1}$, and $e = 0.0$. The peak at 1000 days is quite obvious, and its FAP is 0.0005, resulting in a successful recovery.

4. Results and Discussion

Due to the large number of stars considered here, it is most efficient to present the detection-limit results in terms of the radial-velocity amplitude K which the simulations indicate was detectable. Since the targets in the AAPS long-term program are typically solar-type stars, one can then estimate the mass thresholds by assuming a $1M_{\odot}$ star. Figure 7 shows the distribution of K resulting from the $e = 0.0$ simulations, summed over all stars (123 stars; 12300 K values). As noted in previous work using this detection-limit algorithm (Wittenmyer et al. 2006, 2009, 2010), some injected trial periods can result in apparently undetectable signals, due to poor time sampling or large velocity scatter in the input data. Circular-orbit results are shown in Figure 7, $e = 0.1$ results are shown in Figure 8, and $e = 0.2$ results are shown in Figure 9.

For a given star, the detection limit in K is generally constant over the entire range of trial periods shorter than the duration of observations. Figure 10 shows the detection limit in K for three representative stars. It is useful, then, to compute the mean value of K as the metric of the quality of a star’s detection limit. For each star, we compute the mean K (\bar{K}) and its scatter σ_K , then exclude any values more than $3\sigma_K$ away from that mean and recalculate the mean and its uncertainty. Summed over all stars and all trials, there are

125,100 periods which are shorter than the duration of observations, and a total of 110 K values which were rejected by this $3\sigma_K$ clipping process. The discrepant K values tend to occur at longer periods, especially those longer than the observations. The results are given in Table 2 for all eccentricities and recovery rates. There is a wide range of \bar{K} , spanning two orders of magnitude. This highlights the importance of considering the detection limits on a star-by-star basis. For example, HD 19632, the star for which we obtained the worst detection limits ($\bar{K} > 100\text{m s}^{-1}$), has a chromospheric activity index $\log R'_{HK}$ (Noyes et al. 1984) of -4.38 . This is one of the most active stars on the AAPS target list; “quiet” planet-search target stars typically have $\log R'_{HK} \sim -5.0$. Radial-velocity modulation due to starspots can produce such high levels of jitter (Paulson et al. 2004; Wright 2005), making the determination of meaningful limits extremely difficult. The velocity scatter for the 33 data points on HD 19632 is 26.2m s^{-1} , and the data show a strong periodicity near 6 days, consistent with its estimated rotation period of 12 days (G. Henry, personal communication).

The detection limit achievable from a set of radial-velocity data depends largely on two factors: the number of data points, and their RMS velocity scatter about the mean. Using these results, we can determine an empirical relation between these quantities and the radial-velocity amplitude K which can be detected. Such a relation can then be used to estimate the amount of observing time required to obtain a robust detection (or non-detection) of a particular class of planet. Figure 11 plots the mean K obtained for each star ($e = 0.0$, 99% recovery) versus the quantity RMS/\sqrt{N} . The 119 stars for which $\bar{K} < 50\text{ m s}^{-1}$ were used in a linear fit, yielding the following relation:

$$K = -0.02 + 12.3 \left(\frac{RMS}{\sqrt{N}} \right) \text{ m s}^{-1}. \quad (1)$$

Using this fit, we can make estimates of the number of additional observations required to place robust constraints on planets in the AAPS program. For example, a star with 40 observations at a total velocity rms of 3 m s^{-1} would yield a detection limit of 5.8 m s^{-1} , corresponding to $0.5M_{\text{Jup}}$ ($P = 12\text{ yr}$), and $0.1M_{\text{Jup}}$ ($P = 50\text{ d}$). It is important to note that the cadence of the observations can also have an impact on the types of planets which are or are not detectable. In particular, high-cadence observations are more effective at detecting short-period, low-amplitude planets, as discussed further in the next subsection. We note that recent modifications to the AAPS observing strategy, such as 20-minute integrations to average over stellar oscillation noise, have resulted in velocity rms of $1\text{-}2\text{ m s}^{-1}$ since 2005 for solar-type stars (O’Toole et al. 2009b; Vogt et al. 2010; Wittenmyer et al. 2010). The AAPS plans to obtain a further 6 years of data applying these strategies, which should markedly improve the velocity rms achieved (cf. Table 1), directly resulting in even tighter constraints on Jupiter analogs.

4.1. Known planet hosts

Of the 123 AAPS program targets which (1) have more than 8 years of data, and (2) have more than 30 observations, 25 are known to host at least one planet (plus one brown dwarf host: HD 164427). The planetary parameters are listed in Table 3. A useful sanity check is to ask: “Do the detection-limit results indicate that we could have detected the (known) planet”? That is, we first removed the known planet’s orbit, then added simulated planetary signals to estimate the detectability of a given signal. Applying this method to the planet hosts, then, serves as a simple check of the degree to which this detection-limit method can be trusted. By comparing the velocity amplitude K of the known planets in Table 3 to the \bar{K} detectable for those stars (Table 2), we find that all but four of those planets pass this test at the 99% recovery level: $\bar{K} < K_{planet}$. The four exceptions are: HD 4308b, HD 16417b, HD 23127b, and GJ 832b. For HD 4308 and HD 16417, this result is easily understood by referring to O’Toole et al. (2009b) and O’Toole et al. (2009c). Both of these low-amplitude, short-period planets were only detectable in AAT data during 48-night continuous observing blocks, rather than the several preceding years of more widely-spaced observations. Furthermore, these short-period ($P < 20$ days) planets are wholly different from the Jupiter analogs ($P > 3000$ days) which are the focus of this work. For GJ 832 and HD 23127, we show the detection limit expressed in terms of K as a function of orbital period in Figure 12. In each panel, the known planet is plotted as a large point with error bars. We see that for GJ 832, the detection limit at the *specific* period of the planet is 99%, i.e. the planet has a detectability of 99%, though the *mean* K indicated a detectability of only $\sim 90\%$ (averaged over all periods). Hence, these results are consistent with our robust detection of GJ 832b (Bailey et al. 2009). For HD 23127 (right panel of Figure 12), the planet lies on the 70% recovery contour; this example illustrates that the automated criteria are more conservative than a human investigator (O’Toole et al. 2007). This characteristic of our simulations also applied to the 3 planets orbiting 61 Vir (Vogt et al. 2010), as detailed in Wittenmyer et al. (2010).

4.2. Detectability of Jupiter analogs

In this work, we have adopted the definition of “Jupiter analog” as a giant planet with a long period ($P \gtrsim 8$ yr). By this definition, the AAPS sample includes 3 published Jupiter analogs (HD 134987c, GJ 832b, and HD 160691c³). So, to first order, we have a Jupiter-

³In this paper, we adopt the designation “c” for the outermost planet in the HD 160691 system, after McCarthy et al. (2004)

analog frequency of $3/123 = 2.4\%$. However, this simple calculation assumes that such planets are perfectly detectable for all stars in the sample, which is patently false. As we have computed circular-orbit detection limits at five recovery levels (99, 90, 70, 50, and 10%), we can use these results to apply a rudimentary correction for the relative detectabilities (i.e. the completeness) for each star. Cumming et al. (2008) detailed a similar technique to address the problem of incompleteness for the Keck planet search data. Here, we adopt a simple approach and define the survey completeness for a given radial-velocity amplitude K and period P as:

$$f_c(P_i, K_i) = \frac{1}{N_{stars}} \sum_{j=1}^{N_{stars}} f_{R,j}(P_i, K_i), \quad (2)$$

where $f_R(P, K)$ is the recovery rate as a function of K at period P , and N_{stars} is the total number of stars in the sample ($N = 123$). In this way, we account for the detectabilities for each star individually, at each of the 100 trial periods. We use the specific detection limit K_P obtained for each period from the simulations described above, thus generating five pairs of $(K_P, \text{recovery fraction})$. Then, we generate $f_R(P, K)$ for each star by performing a linear interpolation between the five pairs of $(K_P, \text{recovery fraction})$. We can then estimate the recovery fraction $f_R(P, K)$ for any P and K . As an example, suppose we choose $K = 10 \text{ m s}^{-1}$ and $P = 1000$ days. For HD 10700, which is extremely stable and well-observed, and has very tight detection limits ($\bar{K}_{e=0.0} = 3.7 \text{ m s}^{-1}$), a signal of 10 m s^{-1} would always be detected, and hence $f_R(1000 \text{ days}, 10 \text{ m s}^{-1})$ for HD 10700 is 1.0. For a star with poorer detection limits such as HD 109200 ($\bar{K}_{e=0.0} = 12.3 \text{ m s}^{-1}$), we obtain $f_R(1000 \text{ days}, 10 \text{ m s}^{-1}) = 0.795$. We can see from these examples that if all stars in the sample were stable and well-observed (i.e. if selection effects, observing windows, and velocity jitter were unimportant), then every star would contribute 1.0 to the sum in Equation (2), giving a survey completeness of 1.0 (100%). We could then obtain the planet frequency simply by dividing the number of detections by the total number of stars. However, these effects are extremely important for long-term radial-velocity surveys, and so we use Equation (2) to obtain a more realistic estimate of the completeness of our entire sample as a function of orbital period. Those results are shown in Figure 13. We emphasize that we have *not* included unpublished planet candidates in our estimate of the frequency of Jupiter analogs. In Figure 13, we have summed over 101 stars, excluding 22 stars which exhibited an unusual artefact arising from the ‘‘correct-period’’ criterion discussed in Section 3.2. Consider a data set in which an injected signal with $P_{in} \sim 3500$ days results in $P_{out} = 5000$ days being recovered by the periodogram. For a recovered signal to be accepted, it must be within 27.7% of the injected periodicity. So, for $P_{in} = 3612\text{d}$, $P_{out} = 5000\text{d}$ is rejected, but at $P_{in} = 3671\text{d}$, $P_{out} = 5000\text{d}$ is accepted. This resulted in signals which were ‘‘undetectable’’ even at large K becoming eminently detectable

once P_{in} was within 27.7% of 5000d.

The recovery fraction $f_R(P, K)$ in Equation (2) can be used to derive a completeness correction for the published detections of Jupiter analogs in the AAPS sample. For each of the three stars which hosts a Jupiter analog, we can compute $f_R(P, K)$ at the specific values of P and K for that known planet. As we have computed detection limits for eccentricities of 0.0, 0.1, and 0.2, we used the results from the eccentricity closest to that of each detected planet (GJ 832b: $e = 0.2$, HD 160691c: $e = 0.0$, HD 134987c: $e = 0.1$). This gives the following results: GJ 832 – 0.983; HD 160691 – 1.000; HD 134987 – 1.000. Then, we compute the survey completeness $f_c(P, K)$ to account for the detectability of these specific planets around the 120 remaining stars that do not host a Jupiter analog. Here, $f_c(P, K)$ is computed at the specific values of P and K for each Jupiter analog; those results are then: GJ 832 – 0.685; HD 160691 – 0.863; HD 134987 – 0.440. The frequency of Jupiter analogs based on this sample, corrected for completeness (detectability), is then given by

$$f_{Jup} = \frac{1}{N_{stars}} \sum_{i=1}^{N_{hosts}} \frac{1}{f_{R,i}(P_i, K_i) f_c(P_i, K_i)} = 3.3\%. \quad (3)$$

Here, $N_{stars} = 123$ total stars in the sample, $N_{hosts} = 3$ which host a Jupiter analog, and $f_R(P_i, K_i)$ refers to the recovery fractions listed above. In addition, $f_c(P_i, K_i)$ is summed over the 120 stars which did not host a Jupiter analog, to account for how detectable the three found planets would have been around the remaining stars in the sample.

We can also use the non-detections to compute an upper bound on the frequency of Jupiter analogs in the AAPS sample. Using the recovery fraction $f_R(P, K)$ determined as above for each star at every trial period, we compute the mean of $f_R(P, K)$ over the period range 3000-5000 days. Thus, each of the 120 stars which does *not* host a Jupiter analog has a mean recovery fraction \bar{f}_R , with an uncertainty equal to the standard deviation in $f_R(P, K)$ about that mean. An upper bound on the frequency of Jupiter analogs can then be given by

$$\text{Upper bound} = \frac{1}{N_{nonhosts}} \sum_{i=1}^N 1 - \bar{f}_R, \quad (4)$$

where $N_{nonhosts}$ is the number of stars without a Jupiter analog. The result is an upper bound on the frequency of such planets with K greater than the selected value. Those results are given in Table 4.

Our upper bound of 37% for planets with $K > 10 \text{ ms}^{-1}$ and $e = 0.0$ in the period range 3000-5000 days ($3 \text{ AU} < a < 6 \text{ AU}$) is consistent with the core-accretion simulations of

Liu et al. (2009), in which 83/220 (37%) of systems resulted in at least one planet matching these characteristics. However, our observed frequency of such planets in this sample, 3.3%, is significantly smaller. This difference arises from the simplifying assumptions in the Liu et al. (2009) simulations. First, each simulated system started with a disk mass of 1 minimum-mass solar nebula. A distribution of disk masses may better approximate the formation environments of real planetary systems; Liu et al. are performing further tests with this modification (Huigen Liu, priv. comm.). Second, the simulations proceeded for 10^7 yr; it is possible that subsequent dynamical evolution such as planet-planet scattering events (Rasio & Ford 1996) may eject planets in real systems, which would reduce the observed occurrence rate.

5. Summary and Conclusions

Lineweaver & Grether (2003) addressed the frequency of Jupiter-like planets, defining “Jupiter-like” as those planets with $M_{Saturn} < M \sin i < 3M_{Jup}$ and $3 < a < 9$ AU. Based on the results of eight different Doppler planet surveys, they estimated that $5 \pm 2\%$ of Sun-like stars host Jupiter-like planets. Our estimate of 3.3% is consistent with theirs. We note that this work, unlike that of Lineweaver & Grether (2003), is based on detailed simulations on a star-by-star basis. This approach, while computationally intensive, is critical for a proper characterisation of the selection effects present in radial-velocity data sets (O’Toole et al. 2009c; Wittenmyer et al. 2010).

The comprehensive study on detectabilities from the Keck planet search given in Cumming et al. (2008) focused on planets with periods less than 2000 days ($a \sim 3$ AU for a $1 M_{\odot}$ star). Those authors then extrapolated the simulations results to $a=20$ AU ($P=89$ years). From their Table 2, which gives the giant planet ($M_p > 0.3 M_{Jup}$) occurrence rates for flat and power-law extrapolations, they estimated that $2.7 \pm 0.8\%$ of stars host planets between 3–6 AU. In that range, our measured occurrence rate is $3.3 \pm 1.4\%$. Our results are thus entirely consistent with those of Cumming et al. (2008).

In conclusion, we have performed detailed star-by-star simulations on AAPS data with a time coverage of 12 years, including the effects of eccentricity, in order to make a robust estimate of the frequency of Jupiter analogs in the Solar neighbourhood. Based on our AAPS sample, we calculate that no less than 3.3% and no more than 37.2% of stars host a gas giant planet in a circular orbit between 3–6 AU. We have also performed a comprehensive analysis of the automated detection criteria employed in our simulation method. Salient points arising from this work are (1) the uncertainty in the orbital period of a planet increases dramatically when less than one cycle has been observed, (2) no planet has been published with less than

0.7 cycles of data, and (3) simulating a large number of planet detections reveals that for 99% of planets, the fractional uncertainty in period σ_P/P is 27.7%. This figure is useful for simulations in which one must determine whether an injected signal has been accurately redetected.

We gratefully acknowledge the UK and Australian government support of the Anglo-Australian Telescope through their PPARC, STFC and DIISR funding; STFC grant PP/C000552/1, ARC Grant DP0774000 and travel support from the Anglo-Australian Observatory.

We would like to thank Huigen Liu and Ji-Lin Zhou for helpful details about their simulation results. We thank the AAT TAC for the generous allocation of telescope time to the Anglo-Australian Planet Search. This research has made use of NASA’s Astrophysics Data System (ADS), and the SIMBAD database, operated at CDS, Strasbourg, France. R.W. gratefully acknowledges support from a UNSW Vice-Chancellor’s Fellowship and the UNSW Early-Career Researcher Grants program. This research has made use of the Exoplanet Orbit Database and the Exoplanet Data Explorer at exoplanets.org. We are also grateful to the anonymous referee whose comments greatly improved the clarity of this paper.

REFERENCES

- Bailey, J., Butler, R. P., Tinney, C. G., Jones, H. R. A., O’Toole, S., Carter, B. D., & Marcy, G. W. 2009, *ApJ*, 690, 743
- Baliunas, S., Sokoloff, D., & Soon, W. 1996, *ApJ*, 457, L99
- Barnes, R., & Greenberg, R. 2006, *ApJ*, 638, 478
- Barnes, R., & Greenberg, R. 2006, *ApJ*, 652, L53
- Benedict, G. F., et al. 2006, *AJ*, 132, 2206
- Bouchy, F., et al. 2009, *A&A*, 496, 527
- Butler, R. P., Marcy, G. W., Williams, E., McCarthy, C., Dosanjuh, P., & Vogt, S. S. 1996, *PASP*, 108, 500
- Butler, R. P., Tinney, C. G., Marcy, G. W., Jones, H. R. A., Penny, A. J., & Apps, K. 2001, *ApJ*, 555, 410
- Carter, B. D., Butler, R. P., Tinney, C. G., Jones, H. R. A., Marcy, G. W., McCarthy, C., Fischer, D. A., & Penny, A. J. 2003, *ApJ*, 593, L43

- Cenarro, A. J., et al. 2007, MNRAS, 374, 664
- Chambers, J. E. 1999, MNRAS, 304, 793
- Cochran, W. D., Endl, M., Wittenmyer, R. A., & Bean, J. L. 2007, ApJ, 665, 1407
- Cumming, A., Butler, R. P., Marcy, G. W., Vogt, S. S., Wright, J. T., & Fischer, D. A. 2008, PASP, 120, 531
- Cumming, A., Marcy, G. W., & Butler, R. P. 1999, ApJ, 526, 890
- Diego, F., Charalambous, A., Fish, A. C., & Walker, D. D. 1990, Proc. Soc. Photo-Opt. Instr. Eng., 1235, 562
- Desidera, S., Gratton, R. G., Lucatello, S., Claudi, R. U., & Dall, T. H. 2006, A&A, 454, 553
- Ecuivillon, A., Israelian, G., Santos, N. C., Shchukina, N. G., Mayor, M., & Rebolo, R. 2006, A&A, 445, 633
- Fischer, D. A., et al. 2006, ApJ, 637, 1094
- Fischer, D. A., Marcy, G. W., Butler, R. P., Vogt, S. S., Frink, S., & Apps, K. 2001, ApJ, 551, 1107
- Ford, E. B. 2005, AJ, 129, 1706
- Forveille, T., et al. 2009, A&A, 493, 645
- Gaudi, B. S., et al. 2008, Science, 319, 927
- Gould, A., et al. 2010, arXiv:1001.0572
- Hall, J. C., Lockwood, G. W., & Skiff, B. A. 2007, AJ, 133, 862
- Hatzes, A. P., et al. 2000, ApJ, 544, L145
- Henry, T. J., Soderblom, D. R., Donahue, R. A., & Baliunas, S. L. 1996, AJ, 111, 439
- Howard, A. W., et al. 2009, ApJ, 696, 75
- Jefferys, W. H., Fitzpatrick, M. J., & McArthur, B. E. 1987, Celestial Mechanics, 41, 39
- Jones, H. R. A., Paul Butler, R., Tinney, C. G., Marcy, G. W., Penny, A. J., McCarthy, C., Carter, B. D., & Pourbaix, D. 2002, MNRAS, 333, 871

- Jones, H. R. A., Paul Butler, R., Marcy, G. W., Tinney, C. G., Penny, A. J., McCarthy, C., & Carter, B. D. 2002, MNRAS, 337, 1170
- Jones, H. R. A., Butler, R. P., Tinney, C. G., Marcy, G. W., Penny, A. J., McCarthy, C., & Carter, B. D. 2003, MNRAS, 341, 948
- Jones, H. R. A., Butler, R. P., Tinney, C. G., Marcy, G. W., Carter, B. D., Penny, A. J., McCarthy, C., & Bailey, J. 2006, MNRAS, 369, 249
- Jones, H. R. A., et al. 2010, MNRAS, 403, 1703
- Kürster, M., Schmitt, J. H. M. M., Cutispoto, G., & Dennerl, K. 1997, A&A, 320, 831
- Léger, A., et al. 2009, A&A, 506, 287
- Levison, H. F., & Duncan, M. J. 1994, Icarus, 108, 18
- Lineweaver, C. H., & Grether, D. 2003, ApJ, 598, 1350
- Liu, H., Zhou, J.-l., & Wang, S. 2009, arXiv:0912.1770
- Lomb, N. R. 1976, Ap&SS, 39, 447
- Mayor, M., et al. 2009, A&A, 493, 639
- Mayor, M., et al. 2009, A&A, 507, 487
- McCarthy, C., Butler, R. P., Tinney, C. G., Jones, H. R. A., Marcy, G. W., Carter, B., Penny, A. J., & Fischer, D. A. 2004, ApJ, 617, 575
- Murdoch, K. A., Hearnshaw, J. B., & Clark, M. 1993, ApJ, 413, 349
- Noyes, R. W., Hartmann, L. W., Baliunas, S. L., Duncan, D. K., & Vaughan, A. H. 1984, ApJ, 279, 763
- O’Toole, S. J., et al. 2007, ApJ, 660, 1636
- O’Toole, S. J., Tinney, C. G., & Jones, H. R. A. 2008, MNRAS, 386, 516
- O’Toole, S. J., Tinney, C. G., Jones, H. R. A., Butler, R. P., Marcy, G. W., Carter, B., & Bailey, J. 2009, MNRAS, 392, 641
- O’Toole, S., et al. 2009, ApJ, 697, 1263
- O’Toole, S., et al. 2009, ApJ, 701, 1732

- Paulson, D. B., Saar, S. H., Cochran, W. D., & Henry, G. W. 2004, *AJ*, 127, 1644
- Pepe, F., et al. 2007, *A&A*, 462, 769
- Perryman, M. A. C., et al. 1997, *A&A*, 323, L49
- Rasio, F. A., & Ford, E. B. 1996, *Science*, 274, 954
- Rauch, K. P., & Hamilton, D. P. 2002, *Bulletin of the American Astronomical Society*, 34, 938
- Rivera, E. J., et al. 2005, *ApJ*, 634, 625
- Santos, N. C., Mayor, M., Naef, D., Pepe, F., Queloz, D., Udry, S., & Burnet, M. 2001, *A&A*, 379, 999
- Santos, N. C., et al. 2004, *A&A*, 426, L19
- Scargle, J. D. 1982, *ApJ*, 263, 835
- Sumi, T., et al. 2010, *ApJ*, 710, 1641
- Takeda, G., Ford, E. B., Sills, A., Rasio, F. A., Fischer, D. A., & Valenti, J. A. 2007, *ApJS*, 168, 297
- Tanner, A., Beichman, C., Bryden, G., Lisse, C., & Lawler, S. 2009, *ApJ*, 704, 109
- Tinney, C. G., Butler, R. P., Marcy, G. W., Jones, H. R. A., Penny, A. J., McCarthy, C., & Carter, B. D. 2002, *ApJ*, 571, 528
- Tinney, C. G., Butler, R. P., Marcy, G. W., Jones, H. R. A., Penny, A. J., McCarthy, C., Carter, B. D., & Fischer, D. A. 2005, *ApJ*, 623, 1171
- Tinney, C. G., Butler, R. P., Marcy, G. W., Jones, H. R. A., Penny, A. J., McCarthy, C., Carter, B. D., & Bond, J. 2003, *ApJ*, 587, 423
- Tinney, C. G., Butler, R. P., Marcy, G. W., Jones, H. R. A., Penny, A. J., Vogt, S. S., Apps, K., & Henry, G. W. 2001, *ApJ*, 551, 507
- Trilling, D. E., et al. 2008, *ApJ*, 674, 1086
- Udry, S., et al. 2000, *A&A*, 356, 590
- Udry, S., et al. 2006, *A&A*, 447, 361

- Valenti, J. A., Butler, R. P. & Marcy, G. W. 1995, *PASP*, 107, 966.
- Valenti, J. A., & Fischer, D. A. 2005, *ApJS*, 159, 141
- Vogt, S. S., et al. 2010, *ApJ*, 708, 1366
- Walker, G. A. H., Walker, A. R., Irwin, A. W., Larson, A. M., Yang, S. L. S., & Richardson, D. C. 1995, *Icarus*, 116, 359
- Wittenmyer, R. A., Endl, M., Cochran, W. D., Hatzes, A. P., Walker, G. A. H., Yang, S. L. S., & Paulson, D. B. 2006, *AJ*, 132, 177
- Wittenmyer, R. A., Endl, M., Cochran, W. D., & Levison, H. F. 2007, *AJ*, 134, 1276
- Wittenmyer, R. A., Endl, M., Cochran, W. D., Levison, H. F., & Henry, G. W. 2009, *ApJS*, 182, 97
- Wittenmyer, R. A., O’Toole, S. J., Jones, H. R. A., Tinney, C. G., Butler, R. P., Carter, B. D., & Bailey, J. 2010, *ApJ*, 722, 1854
- Wright, J. T. 2005, *PASP*, 117, 657
- Zhou, J.-L., & Sun, Y.-S. 2003, *ApJ*, 598, 1290

Table 1. Summary of Radial-Velocity Data

Star	N	RMS (m s^{-1})
HD 142	65	17.6 ³
HD 1581	87	3.5
HD 2039	42	15.7 ³
HD 2151	172	4.2
HD 3823	64	5.9
HD 4308	101	4.3 ³
HD 7570	36	6.5
HD 10180	31	6.7
HD 10360	58	4.6 ¹
HD 10361	57	4.3 ¹
HD 10647	35	14.1
HD 10700	209	3.6
HD 11112	30	8.3 ¹
HD 13445	46	21.1 ^{1,3}
HD 16417	103	3.6 ³
HD 19632	33	26.2
HD 20766	37	10.9
HD 20782	40	5.8 ³
HD 20794	121	3.2
HD 20807	81	4.3
HD 23127	38	12.6 ³
HD 27442	74	7.3 ³
HD 28255A	59	7.3 ¹
HD 28255B	39	24.1 ¹
HD 38382	32	5.1
HD 38973	30	4.7
HD 39091	54	5.6 ³
HD 43834	115	5.1
HD 44594	30	5.8
HD 45701	30	5.9 ²
HD 53705	115	4.5
HD 53706	32	2.9
HD 55693	31	7.2
HD 59468	33	5.2
HD 65907a	53	6.5
HD 70642	37	4.8 ³
HD 70889	34	17.6
HD 73121	34	6.2
HD 73524	76	5.2
HD 73526	33	8.0 ³
HD 74868	33	7.8
HD 75289	38	5.9 ³
HD 76700	40	6.4 ³
HD 78429	32	8.9
HD 84117	113	5.5

Table 1—Continued

Star	N	RMS (m s^{-1})
HD 88742	30	12.8
HD 92987	44	5.9 ²
HD 93385	36	6.1
HD 96423	33	5.7
HD 101959	36	6.4
HD 102117	53	4.4 ³
HD 102365	137	3.2
HD 102438	42	4.3
HD 105328	36	5.9
HD 106453	36	11.2
HD 107692	35	11.6
HD 108147	55	19.0
HD 108309	49	3.5
HD 109200	30	4.6
HD 114613	188	5.7
HD 114853	43	5.5
HD 117618	65	5.2 ³
HD 120237	42	10.5
HD 122862	88	4.4
HD 125072	64	5.0
HD 128620	89	3.5 ²
HD 128621	126	3.4 ²
HD 129060	37	37.6
HD 134060	82	5.5
HD 134330	34	5.7
HD 134331	48	5.3 ¹
HD 134606	46	5.3
HD 134987	60	2.5 ³
HD 136352	134	4.6
HD 140901	76	10.3
HD 144628	42	4.0
HD 147722	57	16.8
HD 147723	60	9.1
HD 154577	31	4.4
HD 155974	39	7.5
HD 156274b	88	6.4 ¹
HD 160691	155	2.4 ³
HD 161612	37	3.7
HD 164427	42	6.0 ³
HD 168871	56	4.9
HD 177565	82	4.0
HD 179949	61	11.1 ³
HD 181428	34	7.9
HD 183877	32	5.3
HD 187085	49	5.7 ³

Table 1—Continued

Star	N	RMS (m s^{-1})
HD 189567	73	5.8
HD 190248	187	4.1
HD 191408	153	4.2 ¹
HD 192310	133	4.0
HD 192865	37	11.0
HD 193193	44	5.8
HD 193307	71	4.2
HD 194640	64	4.8
HD 196050	49	7.8 ³
HD 196378	33	6.7
HD 199190	41	3.8
HD 199288	56	5.3
HD 199509	30	6.6 ¹
HD 202560	34	4.9
HD 204385	34	6.8
HD 204961	32	5.7 ³
HD 207129	100	4.9
HD 208487	41	6.0 ³
HD 208998	32	8.4
HD 209653	30	4.4
HD 210918	57	4.6
HD 211317	38	4.3
HD 212168	34	4.9
HD 212708	34	4.1 ¹
HD 213240	33	4.5 ³
HD 214953	72	6.8
HD 216435	69	7.0 ³
HD 216437	46	4.9 ³
HD 217958	30	9.4 ¹
HD 217987	33	8.9
HD 219077	57	5.4 ²
HD 221420	66	4.8 ¹
HD 223171	54	6.3

¹Residuals to a linear fit.

²Residuals to a quadratic fit.

³Residuals after removal of known planet(s) orbit.

Table 2. Summary of Detection Limits

Star	Recovery Rate (percent)	Mean K Detectable (m s^{-1})		
		$e = 0.0$	$e = 0.1$	$e = 0.2$
HD 142	99	24.8±2.4	25.9±2.8	27.8±4.6
	90	23.0±1.5	24.1±2.1	25.1±2.1
	70	18.8±2.4	20.5±2.5	21.7±10.3
	50	15.0±2.2	16.4±1.5	16.7±2.5
HD 1581	99	7.2±9.0	6.4±5.4	6.0±3.3
	90	4.5±1.4	4.9±2.1	5.7±3.6
	70	3.1±0.6	3.5±0.5	3.6±0.8
	50	2.6±1.1	2.8±1.1	3.0±1.4
HD 2039	99	42.6±11.5	45.9±13.1	51.0±13.7
	90	39.2±11.0	39.5±9.7	43.8±15.2
	70	29.9±13.7	34.6±24.4	31.0±9.7
	50	25.0±9.1	24.4±7.4	27.0±9.6
HD 2151	99	6.9±2.9	7.0±1.6	8.0±2.6
	90	6.0±1.2	6.2±1.1	6.4±0.8
	70	5.2±0.8	5.3±0.6	5.5±0.6
	50	4.9±1.4	4.7±0.7	4.8±0.7
HD 3823	99	10.4±3.3	12.2±6.5	12.8±4.9
	90	9.8±4.6	10.2±3.4	10.9±4.7
	70	6.5±1.8	7.3±0.9	7.7±0.9
	50	4.8±2.2	5.0±2.2	5.2±2.3
HD 4308	99	9.1±8.3	9.4±7.7	10.8±8.9
	90	9.4±9.3	8.0±5.2	9.0±6.8
	70	7.0±3.8	7.3±4.2	7.1±3.7
	50	4.9±2.1	5.2±2.1	5.2±1.9
HD 7570	99	13.3±1.2	14.2±1.9	15.6±3.5
	90	11.6±0.8	12.6±1.1	13.1±1.2
	70	9.7±1.0	10.4±0.5	10.9±0.7
	50	8.3±0.9	8.7±0.7	9.1±0.8
HD 10180	99	16.3±3.1	17.2±2.3	19.8±3.4
	90	14.7±2.3	15.5±2.7	17.2±3.6
	70	12.1±1.7	12.8±1.7	14.0±2.7
	50	9.9±2.0	11.0±1.6	11.3±2.2
HD 10360	99	9.5±5.0	9.4±3.9	10.0±3.8
	90	7.7±1.0	8.3±2.3	9.4±6.5
	70	5.9±0.6	6.3±0.8	6.5±0.8
	50	4.5±0.7	4.8±0.6	5.0±0.7
HD 10361	99	7.2±1.2	7.5±0.8	7.8±0.9
	90	6.6±0.5	6.8±0.6	7.1±0.7
	70	5.6±0.5	5.8±0.5	6.0±0.5
	50	4.9±0.5	5.8±0.5	5.2±0.4
HD 10647	99	37.3±7.9	41.6±10.9	43.3±11.2
	90	36.0±9.0	37.6±9.9	40.5±14.7
	70	28.3±4.2	29.9±6.1	32.5±7.2
	50	23.6±4.5	24.5±4.8	26.0±5.2
HD 10700	99	3.7±0.4	4.6±2.9	4.2±0.5

Table 2—Continued

Star	Recovery Rate (percent)	Mean K Detectable (m s^{-1})		
		$e = 0.0$	$e = 0.1$	$e = 0.2$
HD 11112	90	3.4±0.4	3.6±0.4	3.8±0.5
	70	2.1±0.8	2.1±0.8	2.3±0.8
	50	1.6±0.6	1.6±0.5	1.6±0.5
	99	22.7±2.6	26.7±9.1	28.4±2.9
	90	20.4±1.9	22.1±2.5	25.4±4.6
	70	17.5±2.0	18.6±1.5	20.0±2.3
HD 13445	50	14.8±2.4	15.7±2.1	16.8±2.3
	99	41.4±12.4	44.2±13.4	48.2±14.0
	90	37.2±7.6	37.8±6.1	41.8±8.1
	70	33.1±6.8	32.1±4.2	36.5±7.5
HD 16417	50	24.1±5.1	22.5±6.1	23.7±6.3
	99	5.0±1.8	5.5±2.2	6.1±2.1
	90	4.7±1.6	4.8±1.4	5.0±1.4
	70	3.7±0.9	3.8±0.9	3.9±0.8
	50	2.4±0.9	2.8±1.0	2.8±0.9
HD 19632	99	124.1±36.8	126.2±36.2	129.8±36.3
	90	108.8±28.3	111.7±33.2	123.3±48.4
	70	86.5±27.5	88.5±30.6	88.7±23.3
	50	73.0±22.4	87.0±35.4	86.9±29.7
HD 20766	99	23.4±2.1	24.9±2.4	27.6±3.0
	90	21.2±2.4	22.4±1.9	24.0±2.2
	70	12.3±8.5	12.7±8.7	13.4±9.3
	50	9.0±6.8	9.5±7.1	9.9±7.6
HD 20782	99	11.0±1.0	12.0±2.3	12.7±1.1
	90	10.1±0.7	10.6±0.9	11.2±1.2
	70	8.7±0.6	9.1±0.6	9.5±0.6
	50	7.2±1.0	7.8±0.4	8.3±0.6
HD 20794	99	3.9±1.6	4.2±2.2	4.0±1.5
	90	3.3±0.7	3.6±0.9	3.9±1.4
	70	2.6±0.3	2.7±0.3	2.8±0.4
	50	2.3±0.5	2.3±0.4	2.6±1.0
HD 20807	99	8.9±5.0	8.7±3.2	9.2±2.9
	90	7.0±2.0	7.6±2.4	7.8±2.2
	70	4.8±1.1	4.9±0.9	5.2±1.1
	50	3.3±1.1	3.3±1.1	3.3±1.2
HD 23127	99	27.4±2.4	29.4±3.8	32.2±3.9
	90	25.5±2.0	26.3±2.1	28.4±2.5
	70	22.8±1.8	23.3±1.7	24.4±1.8
	50	20.7±1.5	21.2±1.4	22.2±1.4
HD 27442	99	10.0±3.8	9.9±1.2	11.1±1.7
	90	8.7±1.0	9.1±1.2	9.6±1.1
	70	7.4±0.9	7.8±0.7	8.1±1.1
	50	6.2±0.9	6.4±0.8	6.7±0.8
HD 28255A	99	17.5±7.1	18.3±6.8	21.0±10.6
	90	14.0±3.0	15.0±4.2	36.9±21.0

Table 2—Continued

Star	Recovery Rate (percent)	Mean K Detectable (m s^{-1})		
		$e = 0.0$	$e = 0.1$	$e = 0.2$
HD 28255B	70	11.4±3.5	11.7±2.0	11.8±2.0
	50	8.9±2.6	9.4±2.3	9.8±2.7
	99	56.4±11.9	59.5±12.8	65.8±14.7
	90	54.7±13.1	53.5±10.5	58.3±12.0
	70	47.6±7.6	50.9±11.4	53.8±16.7
HD 38382	50	42.1±7.6	47.1±5.8	47.0±8.0
	99	10.4±3.3	12.2±6.5	12.8±4.9
	90	9.8±4.6	10.2±3.4	10.9±4.7
	70	6.5±1.8	7.3±0.9	7.7±0.9
HD 38973	50	4.8±2.2	5.0±2.2	5.2±2.3
	99	13.8±4.1	15.4±2.2	18.2±3.6
	90	11.6±1.1	12.6±1.6	14.0±1.7
	70	9.8±0.6	10.3±1.0	11.0±1.1
HD 39091	50	8.2±0.6	8.7±0.6	9.1±0.6
	99	9.7±3.7	10.3±3.5	10.4±2.1
	90	8.3±1.3	8.7±1.6	9.3±1.8
	70	6.7±0.9	7.3±1.1	7.3±1.0
HD 43834	50	4.9±1.5	5.6±1.1	5.9±1.2
	99	8.8±4.5	9.3±6.0	9.9±6.6
	90	7.5±1.8	7.9±2.3	8.5±3.1
	70	6.2±1.5	6.6±1.6	6.9±1.7
	50	4.2±1.2	4.5±1.0	4.8±1.0
HD 44594	99	16.2±5.5	16.3±1.9	18.3±2.1
	90	13.7±2.2	14.8±2.6	15.4±1.5
	70	11.7±1.0	12.8±1.6	13.7±3.0
	50	10.4±0.6	10.9±0.8	11.6±1.0
HD 45701	99	22.7±9.9	24.6±7.1	26.2±7.5
	90	19.5±6.1	22.6±11.1	21.1±7.0
	70	15.3±4.2	16.3±4.1	17.0±4.4
	50	12.5±1.9	13.0±1.9	13.8±2.1
HD 53705	99	6.0±1.4	6.3±1.2	6.8±1.1
	90	5.9±1.7	6.1±2.3	6.4±1.9
	70	5.3±1.0	5.5±1.1	5.9±1.4
	50	4.4±0.5	4.6±0.6	4.8±0.6
HD 53706	99	6.0±0.5	6.7±0.7	7.7±1.5
	90	5.5±0.2	5.7±0.3	6.2±0.4
	70	4.9±0.3	5.1±0.3	5.4±0.3
	50	4.4±0.4	4.6±0.3	4.8±0.3
HD 55693	99	18.5±2.7	20.6±3.5	24.7±6.2
	90	16.6±2.3	17.8±2.4	19.8±3.0
	70	13.9±1.8	14.8±1.5	15.9±1.6
	50	11.8±2.1	12.5±1.9	13.3±2.2
HD 59468	99	11.4±1.2	12.1±1.3	13.4±1.4
	90	10.1±0.7	10.6±0.9	11.4±0.9
	70	8.4±0.8	9.1±0.5	9.7±0.5

Table 2—Continued

Star	Recovery Rate (percent)	Mean K Detectable (m s^{-1})		
		$e = 0.0$	$e = 0.1$	$e = 0.2$
HD 65907a	50	7.0±1.2	7.4±1.0	7.8±1.1
	99	10.1±1.5	10.8±1.6	11.8±2.2
	90	8.8±1.0	9.6±1.5	10.1±1.5
	70	6.0±1.8	7.1±0.8	7.5±0.7
HD 70642	50	4.3±2.0	4.4±2.1	4.6±2.1
	99	10.0±1.0	11.2±2.0	12.0±1.7
	90	8.8±0.7	9.5±0.9	10.3±1.0
	70	7.4±0.6	7.8±0.5	8.2±0.7
HD 70889	50	6.5±0.6	6.8±0.4	7.2±0.3
	99	58.5±25.7	59.7±21.6	74.2±29.8
	90	51.1±17.4	54.2±21.2	58.4±20.9
	70	39.6±7.6	41.6±9.1	45.1±10.9
HD 73121	50	31.9±8.0	32.4±6.3	33.4±5.7
	99	12.3±1.1	13.3±0.9	15.1±2.7
	90	11.1±0.5	11.7±0.7	12.7±0.7
	70	9.7±1.0	10.0±0.6	10.7±0.8
HD 73524	50	8.6±1.2	8.9±1.0	9.4±1.0
	99	10.7±4.0	11.7±4.5	12.2±3.3
	90	8.8±1.8	9.3±2.0	10.3±3.7
	70	6.9±0.9	7.3±0.7	7.8±0.9
HD 73526	50	5.2±0.8	5.5±0.8	5.7±0.8
	99	22.8±6.2	25.3±8.3	29.1±11.0
	90	19.5±3.4	21.4±5.1	23.6±6.7
	70	17.8±3.1	18.6±4.1	19.2±3.0
HD 74868	50	15.2±1.4	15.8±1.8	16.9±2.6
	99	18.0±1.6	19.4±2.1	21.8±3.1
	90	16.2±1.3	17.2±1.4	18.7±1.7
	70	12.9±2.2	14.3±1.4	14.8±1.7
HD 75289	50	9.5±3.6	10.2±3.4	10.9±3.6
	99	11.4±1.0	12.3±1.4	13.8±1.6
	90	10.5±0.7	11.1±0.8	11.9±1.0
	70	8.7±1.0	9.6±1.0	9.8±1.1
HD 76700	50	7.3±1.3	8.0±1.4	8.4±1.5
	99	14.3±2.0	16.3±4.3	17.6±3.7
	90	13.4±1.8	13.9±2.0	15.1±2.4
	70	12.2±4.4	11.4±2.1	12.4±2.3
HD 78429	50	9.9±3.2	10.2±3.4	10.6±3.6
	99	13.3±1.2	14.2±1.9	15.6±3.5
	90	11.6±0.8	12.6±1.1	13.1±1.2
	70	9.7±1.0	10.4±0.5	10.9±0.7
HD 84117	50	8.3±0.9	8.7±0.7	9.1±0.8
	99	8.4±2.9	8.9±3.5	9.1±3.3
	90	7.4±1.2	7.8±1.4	8.3±1.9
	70	6.4±1.0	6.8±1.0	7.2±1.1
	50	5.8±0.8	6.0±0.8	6.3±0.9

Table 2—Continued

Star	Recovery Rate (percent)	Mean K Detectable (m s^{-1})		
		$e = 0.0$	$e = 0.1$	$e = 0.2$
HD 88742	99	31.0±1.5	33.8±2.6	40.5±9.1
	90	28.5±1.1	29.9±1.5	32.9±2.6
	70	23.5±3.0	24.5±2.5	26.4±2.9
	50	16.2±5.7	17.7±5.1	18.8±5.5
HD 92987	99	9.6±0.6	10.2±1.0	10.5±0.7
	90	8.9±0.5	9.1±0.4	9.7±0.8
	70	8.1±0.4	8.2±0.3	8.8±0.3
	50	7.2±0.3	7.3±0.3	7.9±0.5
HD 93385	99	13.4±1.3	14.9±1.8	17.1±3.0
	90	11.9±1.1	12.7±1.1	13.9±1.5
	70	9.9±1.0	10.5±0.6	11.2±1.1
	50	8.7±1.5	9.1±1.3	9.5±1.3
HD 96423	99	12.8±1.0	13.5±1.2	16.3±4.7
	90	11.6±0.8	12.4±0.8	13.2±0.9
	70	10.4±0.5	10.9±0.4	11.5±0.5
	50	9.5±0.5	9.9±0.4	10.4±0.4
HD 101959	99	13.2±1.2	14.3±1.5	16.0±1.8
	90	11.9±0.9	11.9±0.9	13.7±1.2
	70	10.5±0.7	10.5±0.7	10.9±0.6
	50	9.1±0.6	9.5±0.7	9.9±0.6
HD 102117	99	7.0±0.7	7.6±0.9	8.5±0.6
	90	6.6±0.5	6.7±0.5	7.3±0.6
	70	6.1±0.7	6.2±1.0	6.4±0.9
	50	5.4±0.7	5.4±0.5	5.7±0.6
HD 102365	99	3.8±0.7	4.1±1.0	4.9±1.9
	90	3.5±0.7	3.7±0.7	4.1±1.2
	70	3.1±0.6	3.4±0.7	3.5±0.7
	50	2.4±0.4	2.6±0.2	2.7±0.3
HD 102438	99	7.5±0.8	8.0±1.3	9.3±3.9
	90	6.8±0.8	7.3±0.8	7.5±1.3
	70	5.1±0.6	5.8±0.6	5.8±0.7
	50	3.8±0.7	4.2±0.5	4.3±0.6
HD 105328	99	11.5±0.9	12.3±1.0	13.6±2.1
	90	10.5±0.6	10.9±0.6	11.8±0.8
	70	8.9±0.8	9.5±0.3	9.8±0.6
	50	7.5±1.3	7.9±1.1	8.2±1.2
HD 106453	99	24.1±6.0	25.5±3.1	29.0±3.7
	90	22.1±3.9	23.2±4.1	23.8±1.4
	70	19.0±3.0	19.4±2.1	21.4±4.4
	50	17.0±2.7	18.9±5.6	20.8±8.7
HD 107692	99	29.2±8.3	29.0±2.4	32.5±3.7
	90	24.8±4.2	26.8±4.6	29.5±6.7
	70	17.8±3.8	19.7±4.1	20.5±4.6
	50	14.8±3.2	15.4±3.1	16.4±3.3
HD 108147	99	42.5±10.4	44.0±8.7	49.5±10.4

Table 2—Continued

Star	Recovery Rate (percent)	Mean K Detectable (m s^{-1})		
		$e = 0.0$	$e = 0.1$	$e = 0.2$
HD 108309	90	41.7±15.0	40.2±8.1	42.1±6.5
	70	41.7±22.4	34.5±8.5	36.0±6.3
	50	31.5±6.4	33.4±7.0	35.6±7.9
	99	5.4±0.8	5.6±1.3	5.7±0.7
	90	4.9±0.4	5.2±0.5	5.9±3.1
	70	4.1±0.3	4.3±0.3	4.3±0.3
HD 109200	50	3.5±0.4	3.7±0.4	3.8±0.5
	99	12.3±1.0	13.6±1.5	16.4±4.8
	90	10.7±0.7	11.4±0.7	12.9±1.1
	70	9.5±0.6	9.8±0.4	10.6±0.4
HD 114613	50	8.3±0.5	8.6±0.4	9.3±0.4
	99	7.5±3.7	7.9±4.1	8.5±4.3
	90	6.8±3.3	7.1±3.5	7.2±3.4
	70	5.4±2.4	5.5±2.5	5.6±2.5
HD 114853	50	4.4±1.9	4.4±1.8	4.6±1.9
	99	9.1±0.7	9.5±0.8	10.5±0.9
	90	8.5±0.5	8.9±0.6	9.3±0.3
	70	7.5±0.5	7.9±0.4	8.3±0.5
HD 117618	50	6.6±0.8	7.1±0.5	7.2±0.7
	99	7.8±1.4	8.5±2.3	10.0±5.5
	90	7.4±1.4	7.5±0.9	8.1±1.4
	70	6.1±1.0	6.3±1.3	7.1±1.8
HD 120237	50	4.7±1.3	4.9±1.4	5.4±1.4
	99	18.9±2.0	20.0±2.4	21.6±2.8
	90	17.2±1.5	18.2±1.9	19.3±2.0
	70	14.2±1.7	15.1±1.0	15.7±1.2
HD 122862	50	11.9±2.3	12.5±1.5	12.8±1.9
	99	8.3±6.4	7.8±3.8	8.0±3.0
	90	6.5±2.5	6.5±1.9	6.6±1.7
	70	5.0±0.8	5.1±0.7	5.3±0.5
HD 125072	50	4.4±0.7	4.5±0.5	4.7±0.5
	99	8.7±1.2	9.3±1.3	9.9±1.3
	90	7.2±1.9	8.1±1.0	8.4±1.0
	70	5.1±2.1	5.7±2.0	5.6±1.9
HD 128620	50	3.3±2.0	3.8±2.0	3.6±2.0
	99	6.4±2.2	7.5±3.6	9.2±7.5
	90	5.2±1.7	5.4±1.4	6.0±2.0
	70	3.6±1.1	3.9±1.1	4.0±1.3
HD 128621	50	2.3±1.1	3.1±1.1	2.7±1.0
	99	6.2±1.1	6.9±1.6	8.1±3.7
	90	5.5±0.8	5.7±1.0	6.1±1.1
	70	4.2±0.7	4.2±0.7	4.4±0.7
HD 129060	50	3.1±1.0	2.9±1.0	3.1±0.9
	99	98.2±21.5	104.6±24.3	116.8±28.4
	90	97.2±25.9	93.7±16.2	101.9±17.3

Table 2—Continued

Star	Recovery Rate (percent)	Mean K Detectable (m s^{-1})		
		$e = 0.0$	$e = 0.1$	$e = 0.2$
HD 134060	70	79.8±14.6	81.8±16.8	87.2±17.6
	50	75.8±24.1	76.7±21.5	85.8±26.5
	99	9.5±6.3	9.6±3.5	10.2±2.9
	90	7.6±2.6	7.9±1.7	8.2±1.3
	70	5.6±0.8	6.0±0.7	6.2±0.7
HD 134330	50	4.4±1.1	4.8±1.0	4.7±1.1
	99	12.9±1.3	13.9±1.8	15.2±1.7
	90	11.6±1.1	12.3±1.3	13.3±1.7
	70	10.1±0.8	10.5±0.7	11.0±0.9
HD 134331	50	8.3±0.7	8.6±0.8	9.4±0.7
	99	9.4±4.5	9.2±0.5	9.8±0.7
	90	8.6±2.3	9.0±2.4	8.8±0.4
	70	7.2±0.5	7.6±0.9	7.9±1.0
HD 134606	50	6.0±0.8	6.5±0.8	6.6±0.7
	99	8.8±1.8	9.3±2.3	9.7±0.8
	90	7.7±0.7	8.1±1.0	8.4±0.5
	70	6.6±0.7	7.1±0.6	7.5±0.8
HD 134987	50	5.8±0.6	6.1±0.6	6.3±0.6
	99	3.8±0.4	4.1±0.5	4.4±0.7
	90	3.4±0.4	3.6±0.4	3.8±0.4
	70	2.8±0.5	3.0±0.5	3.1±0.6
	50	2.3±0.7	2.4±0.8	2.6±0.8
HD 136352	99	7.0±3.3	6.9±1.1	7.7±1.9
	90	6.1±1.4	7.0±3.6	6.5±0.8
	70	5.0±0.6	5.4±0.7	5.7±0.8
	50	4.3±0.3	4.7±0.5	4.8±0.5
HD 140901	99	19.0±8.2	18.5±4.6	20.6±7.1
	90	17.2±4.5	18.3±7.4	18.1±5.2
	70	13.3±2.3	13.5±2.4	14.1±2.6
	50	9.8±2.8	9.8±3.6	10.4±3.1
HD 144628	99	7.1±1.3	7.3±0.7	8.1±1.1
	90	6.5±0.4	6.7±0.4	7.1±0.5
	70	5.6±0.4	6.0±0.6	6.1±0.5
	50	4.7±0.4	5.0±0.3	5.2±0.3
HD 147722	99	25.4±2.2	26.5±2.8	28.8±3.9
	90	23.9±1.8	24.5±2.2	25.3±2.5
	70	22.9±10.0	21.1±1.0	21.7±1.3
	50	19.2±2.0	19.6±1.9	20.5±2.1
HD 147723	99	15.3±2.1	15.9±2.4	17.1±2.6
	90	14.2±1.9	14.8±2.1	15.5±2.5
	70	11.9±1.2	12.4±1.2	13.0±1.6
	50	9.9±1.6	10.5±1.4	11.1±1.6
HD 154577	99	9.9±0.7	10.8±1.3	12.7±3.7
	90	9.0±0.6	9.6±0.8	10.5±1.1
	70	7.9±0.7	8.4±0.6	9.0±0.8

Table 2—Continued

Star	Recovery Rate (percent)	Mean K Detectable (m s^{-1})		
		$e = 0.0$	$e = 0.1$	$e = 0.2$
HD 155974	50	7.1±0.7	7.4±0.6	7.9±0.8
	99	14.4±1.0	15.3±1.2	16.8±1.7
	90	13.4±0.8	13.9±0.8	14.9±1.1
	70	12.1±1.3	12.5±1.2	13.8±3.5
HD 156274b	50	10.8±1.2	11.1±0.9	11.9±1.8
	99	12.2±9.4	13.6±10.3	16.9±17.0
	90	8.3±2.7	9.4±3.7	10.9±6.3
	70	6.3±1.5	7.1±1.0	7.2±1.3
HD 160691	50	5.3±1.7	5.5±1.5	5.7±1.6
	99	2.3±0.3	2.6±0.9	2.8±1.1
	90	2.0±0.2	2.2±0.2	2.3±0.4
	70	1.8±0.4	1.8±0.2	1.9±0.2
HD 161612	50	1.5±0.2	1.6±0.2	1.6±0.4
	99	7.1±0.5	7.5±0.7	8.6±0.9
	90	6.7±0.7	6.9±0.4	7.2±0.4
	70	5.8±0.7	6.4±0.7	6.5±1.2
HD 164427	50	5.3±0.5	5.5±0.5	5.7±0.6
	99	15.9±8.5	18.0±17.5	13.9±3.1
	90	12.6±3.6	13.9±4.5	16.0±6.2
	70	11.5±6.4	13.0±6.7	13.5±8.0
HD 168871	50	13.4±10.4	11.9±5.0	12.8±6.8
	99	10.4±8.4	10.8±7.5	11.1±7.1
	90	8.9±4.4	9.2±4.9	8.9±3.4
	70	5.4±2.1	6.4±1.7	6.5±3.1
HD 177565	50	3.3±1.6	3.7±1.7	3.9±1.9
	99	7.9±5.0	7.1±1.5	7.6±1.4
	90	6.6±2.8	6.5±1.2	6.9±1.6
	70	3.6±1.8	3.7±1.9	4.1±1.8
HD 179949	50	2.3±1.5	2.4±1.5	2.5±1.5
	99	21.8±11.1	20.9±6.4	22.1±4.6
	90	19.1±5.6	20.8±9.3	19.5±2.6
	70	15.3±2.6	15.4±2.8	16.9±2.6
HD 181428	50	11.1±2.4	9.9±2.2	12.2±2.5
	99	18.4±1.8	19.8±2.1	22.1±3.1
	90	16.8±1.3	17.4±1.2	18.6±1.3
	70	14.2±1.1	15.5±1.8	15.9±2.5
HD 183877	50	12.5±1.1	12.9±1.0	13.8±1.3
	99	12.5±1.7	14.0±2.6	16.2±4.0
	90	11.6±1.9	12.1±2.4	13.6±5.9
	70	9.9±1.0	10.6±1.4	11.4±2.3
HD 187085	50	8.6±1.0	9.1±1.1	9.7±1.4
	99	8.9±0.6	9.2±0.6	9.9±1.0
	90	8.4±0.5	8.7±0.5	9.0±0.5
	70	7.5±0.9	7.5±0.2	7.8±0.4
	50	6.8±0.5	7.1±0.7	7.3±0.4

Table 2—Continued

Star	Recovery Rate (percent)	Mean K Detectable (m s^{-1})		
		$e = 0.0$	$e = 0.1$	$e = 0.2$
HD 189567	99	10.5±4.2	10.4±3.2	11.2±3.1
	90	8.5±2.0	9.0±2.2	9.5±3.0
	70	7.0±1.3	7.6±1.2	7.8±1.3
	50	5.9±1.9	6.4±1.3	6.6±1.6
HD 190248	99	4.9±1.4	5.6±2.7	5.8±2.1
	90	4.3±0.9	4.5±0.9	4.8±1.2
	70	3.5±0.5	3.8±0.7	4.0±0.6
HD 191408	99	4.4±0.7	4.7±0.8	5.1±0.8
	90	4.1±0.6	4.2±0.6	4.5±0.6
	70	3.4±0.3	3.5±0.2	3.7±0.3
HD 192310	99	2.8±0.3	2.9±0.2	3.0±0.3
	99	3.4±1.8	3.6±1.9	3.8±2.0
	90	3.1±1.6	3.2±1.7	3.4±1.7
HD 192865	70	2.6±1.3	2.7±1.3	2.8±1.4
	50	2.4±1.2	2.4±1.3	2.5±1.3
	99	28.4±6.9	31.2±8.6	35.9±11.0
	90	26.3±6.2	27.8±6.6	32.5±11.4
HD 193193	70	21.8±3.4	23.0±3.1	24.4±3.6
	50	17.9±3.0	19.5±2.7	19.7±3.4
	99	17.1±14.5	18.4±15.5	19.5±17.5
	90	15.0±10.8	16.7±14.5	17.4±14.8
HD 193307	70	13.1±12.3	12.8±11.5	11.0±4.3
	50	9.0±3.2	8.9±2.0	9.9±3.6
	99	9.4±7.6	9.2±4.0	11.0±6.0
	90	7.0±2.6	6.8±1.6	6.8±1.4
HD 194640	70	5.1±0.8	5.2±0.8	5.4±0.9
	50	4.2±1.0	4.4±0.8	4.4±0.9
	99	10.4±9.1	8.9±3.3	8.7±1.3
	90	7.4±1.1	7.5±0.7	7.9±0.8
HD 196050	70	6.5±0.7	6.6±0.8	6.9±0.9
	50	6.2±1.0	6.3±0.9	6.5±1.0
	99	13.6±1.7	14.3±2.0	15.7±1.9
	90	12.9±1.4	13.4±1.7	13.9±1.6
HD 196378	70	11.6±1.8	12.1±1.2	12.2±1.1
	50	9.5±1.3	10.9±1.5	11.2±3.0
	99	15.3±1.1	16.8±1.6	18.7±1.1
	90	14.0±0.9	15.0±1.1	16.4±1.7
HD 199190	70	12.7±1.9	13.2±0.8	14.1±1.1
	50	12.0±1.7	12.3±1.6	13.1±1.9
	99	6.8±0.6	7.2±1.6	7.7±0.5
	90	6.4±0.5	6.6±0.5	7.1±0.6
HD 199288	70	5.9±0.7	6.1±0.9	6.1±0.4
	50	5.5±0.6	5.7±1.0	5.7±0.5
	99	10.2±1.4	10.7±1.4	11.4±1.6

Table 2—Continued

Star	Recovery Rate (percent)	Mean K Detectable (m s^{-1})		
		$e = 0.0$	$e = 0.1$	$e = 0.2$
HD 199509	90	9.2±1.1	9.6±1.2	10.2±1.4
	70	7.5±1.0	7.8±0.9	8.2±1.2
	50	6.8±1.2	6.9±1.1	7.3±1.2
	99	25.7±10.6	29.4±14.7	33.7±19.8
	90	23.1±10.0	22.7±8.7	23.7±8.8
HD 202560	70	15.9±3.3	16.7±4.2	21.1±9.3
	50	13.3±2.4	13.4±2.3	15.7±4.7
	99	10.6±1.0	11.4±1.2	12.4±1.5
	90	9.7±0.7	10.0±0.7	11.0±1.2
	70	8.2±0.5	8.5±0.4	8.9±0.3
HD 204385	50	6.9±0.7	7.2±0.4	7.5±0.6
	99	14.6±0.7	15.7±0.8	17.9±2.2
	90	13.5±0.7	14.1±0.5	15.4±0.8
	70	11.3±1.8	11.9±0.9	12.5±1.2
	50	9.1±1.7	9.6±1.6	10.0±1.7
HD 204961	99	14.0±4.7	14.9±1.8	16.7±2.2
	90	12.8±1.4	13.2±1.5	14.2±1.3
	70	11.4±0.9	11.8±0.9	12.7±1.1
	50	10.3±0.6	10.7±0.6	11.2±0.8
	99	8.7±1.2	9.3±1.4	10.3±1.7
HD 207129	90	7.5±1.1	8.0±1.1	8.6±1.1
	70	5.9±0.9	6.2±0.8	6.3±0.7
	50	4.7±1.0	4.8±0.5	5.0±0.7
	99	11.1±1.2	12.1±1.6	13.9±2.2
	90	10.0±0.8	11.0±1.9	11.4±1.0
HD 208487	70	9.2±0.6	9.6±0.6	10.2±0.7
	50	8.6±0.8	9.0±1.0	9.1±0.6
	99	18.9±1.9	20.9±5.0	24.4±11.3
	90	17.4±1.2	18.3±1.6	20.2±3.0
	70	16.4±1.6	17.1±2.5	18.1±3.0
HD 208998	50	15.2±1.3	15.5±1.7	16.1±1.4
	99	10.6±0.9	12.7±6.0	12.9±0.8
	90	9.8±0.7	10.2±1.0	11.4±1.8
	70	8.8±1.1	9.1±1.3	9.7±0.7
	50	8.3±1.2	8.5±1.5	9.0±1.4
HD 210918	99	13.6±11.1	14.5±12.3	15.9±9.7
	90	13.5±11.8	13.0±9.5	14.6±11.1
	70	6.9±3.7	7.5±4.3	7.7±4.3
	50	4.6±3.0	4.7±3.1	5.0±3.3
	99	10.4±3.7	10.8±2.6	11.7±1.8
HD 211317	90	8.6±1.4	9.0±1.1	9.8±1.1
	70	7.3±0.8	7.7±0.7	8.1±1.2
	50	6.4±0.9	6.7±0.8	7.1±1.0
	99	10.6±0.7	11.7±0.7	12.9±1.0
	90	9.7±0.6	10.2±0.3	10.9±0.5

Table 2—Continued

Star	Recovery Rate (percent)	Mean K Detectable (m s^{-1})		
		$e = 0.0$	$e = 0.1$	$e = 0.2$
HD 212708	70	8.4±0.5	9.0±1.0	9.6±1.4
	50	7.6±0.5	7.9±0.6	8.3±0.8
	99	13.1±4.3	15.6±6.0	21.9±13.0
	90	12.4±5.6	11.5±3.8	12.6±4.5
HD 213240	70	9.6±2.7	11.7±4.1	12.7±5.7
	50	7.6±1.3	8.1±1.4	8.6±1.6
	99	16.5±7.8	19.1±9.3	21.2±9.6
	90	12.5±3.0	14.1±4.4	15.4±4.7
HD 214953	70	11.3±3.3	13.5±5.1	14.7±6.2
	50	9.1±1.3	10.0±2.0	10.8±2.4
	99	19.8±17.1	18.7±13.1	18.2±8.6
	90	11.8±3.1	14.0±3.7	13.1±5.4
HD 216435	70	9.0±6.5	8.7±4.2	8.8±4.3
	50	7.3±3.3	7.4±3.4	7.7±3.5
	99	8.5±0.5	8.9±0.7	10.1±2.1
	90	8.3±0.5	8.4±0.5	8.7±0.6
HD 216437	70	7.7±0.7	7.7±0.9	8.2±1.0
	50	6.9±0.6	7.0±0.7	7.3±0.8
	99	8.4±0.9	9.0±1.3	10.4±3.1
	90	7.5±0.6	8.0±0.6	8.4±0.8
HD 217958	70	6.7±0.8	7.2±1.8	7.3±1.0
	50	6.0±0.6	6.3±0.5	6.6±0.6
	99	32.3±7.3	36.0±9.1	43.8±14.7
	90	30.7±11.7	30.0±6.5	35.3±9.8
HD 217987	70	27.6±7.8	26.8±6.8	31.9±10.0
	50	23.3±5.4	23.4±4.9	26.2±6.8
	99	22.0±3.8	24.0±4.9	27.5±6.2
	90	20.1±2.5	21.0±3.0	22.8±3.4
HD 219077	70	18.6±3.2	18.2±1.3	19.6±1.6
	50	16.6±1.5	17.0±1.5	18.1±2.4
	99	13.5±8.2	14.0±7.5	15.5±8.8
	90	9.5±2.8	10.6±3.4	11.0±3.9
HD 221420	70	6.3±2.2	7.1±1.7	7.1±2.4
	50	4.0±2.4	4.0±2.5	4.2±2.6
	99	12.3±8.2	14.2±12.1	14.2±9.5
	90	8.2±1.7	9.9±4.1	10.3±4.1
HD 223171	70	5.2±2.2	6.1±1.5	6.6±4.1
	50	4.4±2.2	4.7±2.2	4.9±2.3
	99	9.1±1.5	10.3±2.9	12.8±8.5
	90	8.1±0.8	8.6±1.0	9.5±1.5
	70	7.2±1.8	7.4±0.7	7.5±0.9
	50	5.9±1.0	6.5±1.6	6.9±2.2

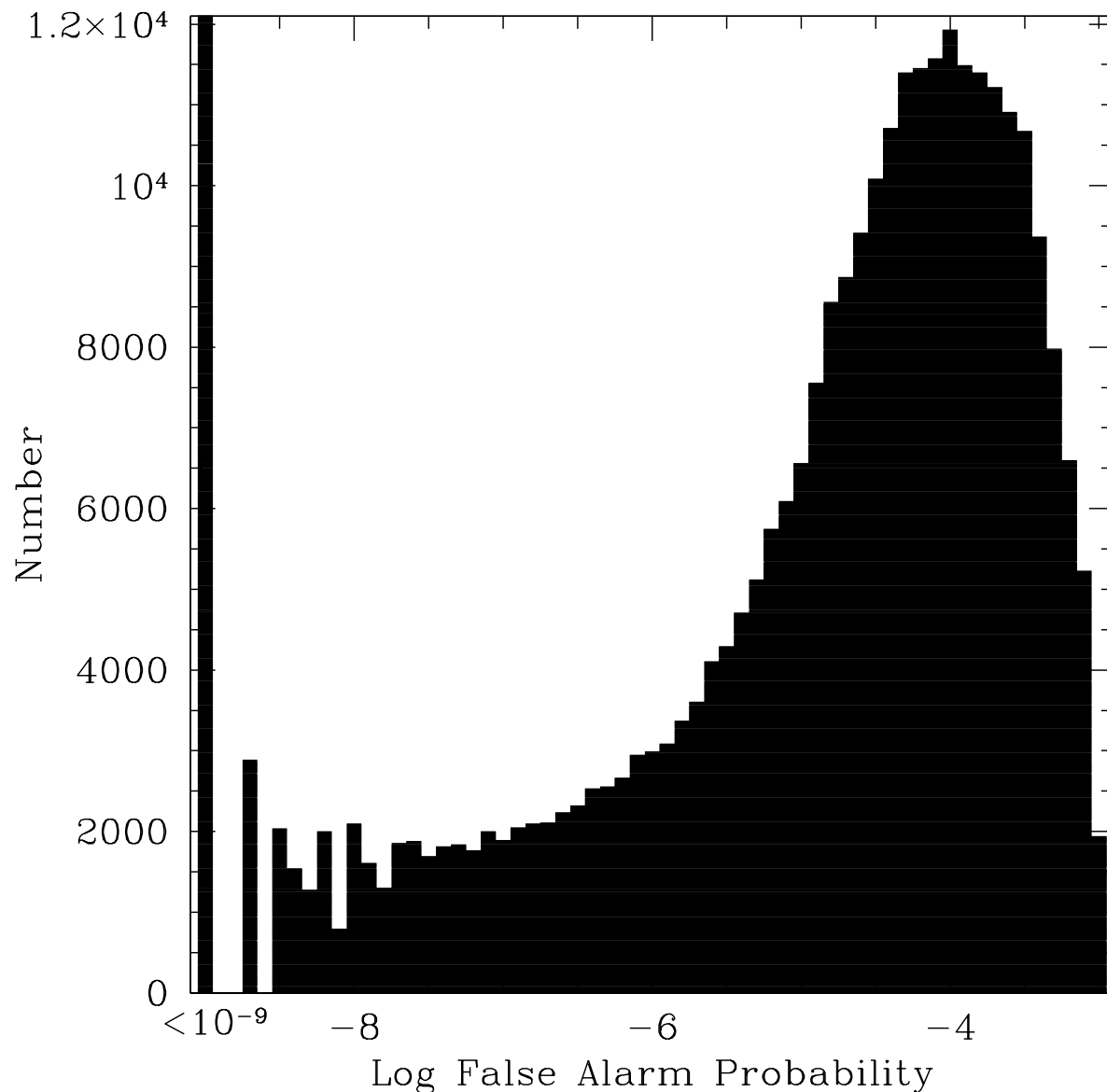


Fig. 1.— Distribution of false-alarm probabilities for 362368 successfully recovered signals from detection-limit simulations for 123 stars ($e = 0.0$, 99% recovery). Though the cutoff criterion was 0.001, the vast majority of signals were recovered at greater significance, and 18.4% of signals were recovered with $\text{FAP} < 10^{-9}$. Of all trial signals, 23.0% were rejected based on the FAP cutoff criterion.

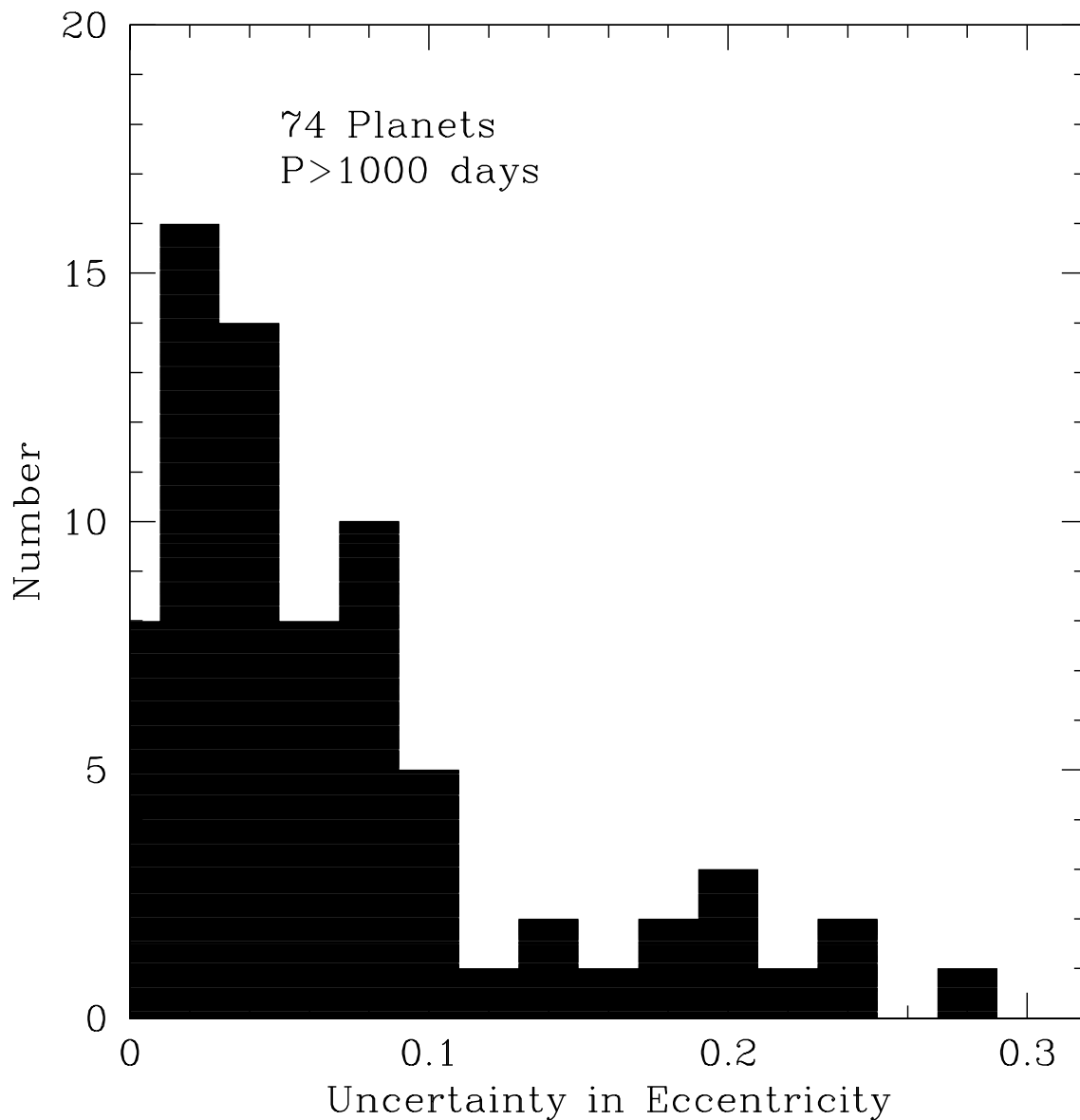


Fig. 2.— Distribution of the published uncertainties in eccentricity for the 74 published long-period planets ($P > 1000$ days) based on exoplanet.eu, 2010 September 1. The distribution peaks in the range $\sigma_e = 0.02$ - 0.04 ; the true uncertainty in eccentricity may be considerably larger due to non-Gaussianities as described in Ford (2005) and O’Toole et al. (2009a).

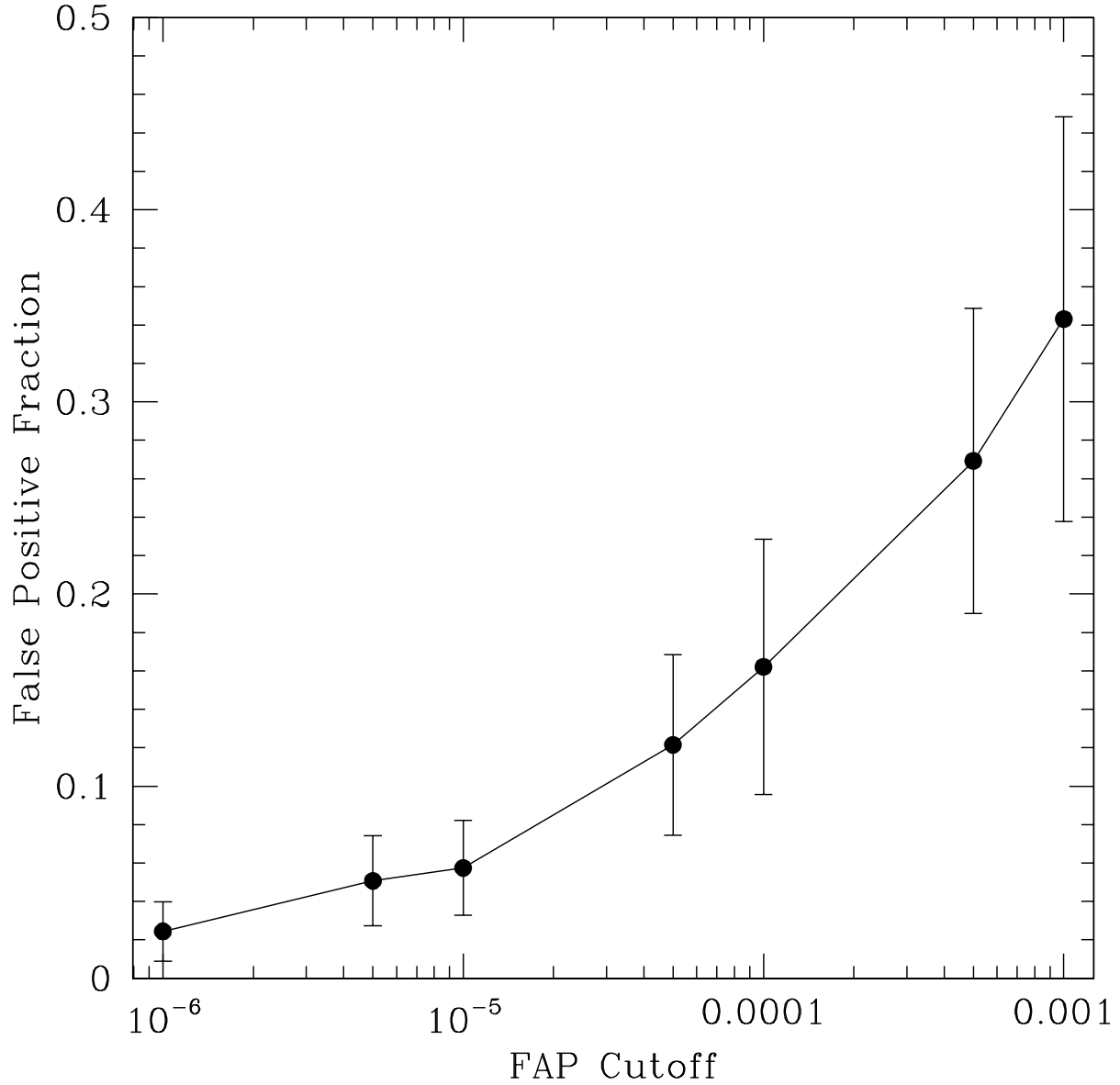


Fig. 3.— Mean false positive rate obtained from tests of the detection-limit routine in which the correct-period criterion was removed. Incorrectly recovered periods tend to have higher FAPs, and should be excluded, but a nontrivial number of false positives occur even at extremely stringent FAP levels.

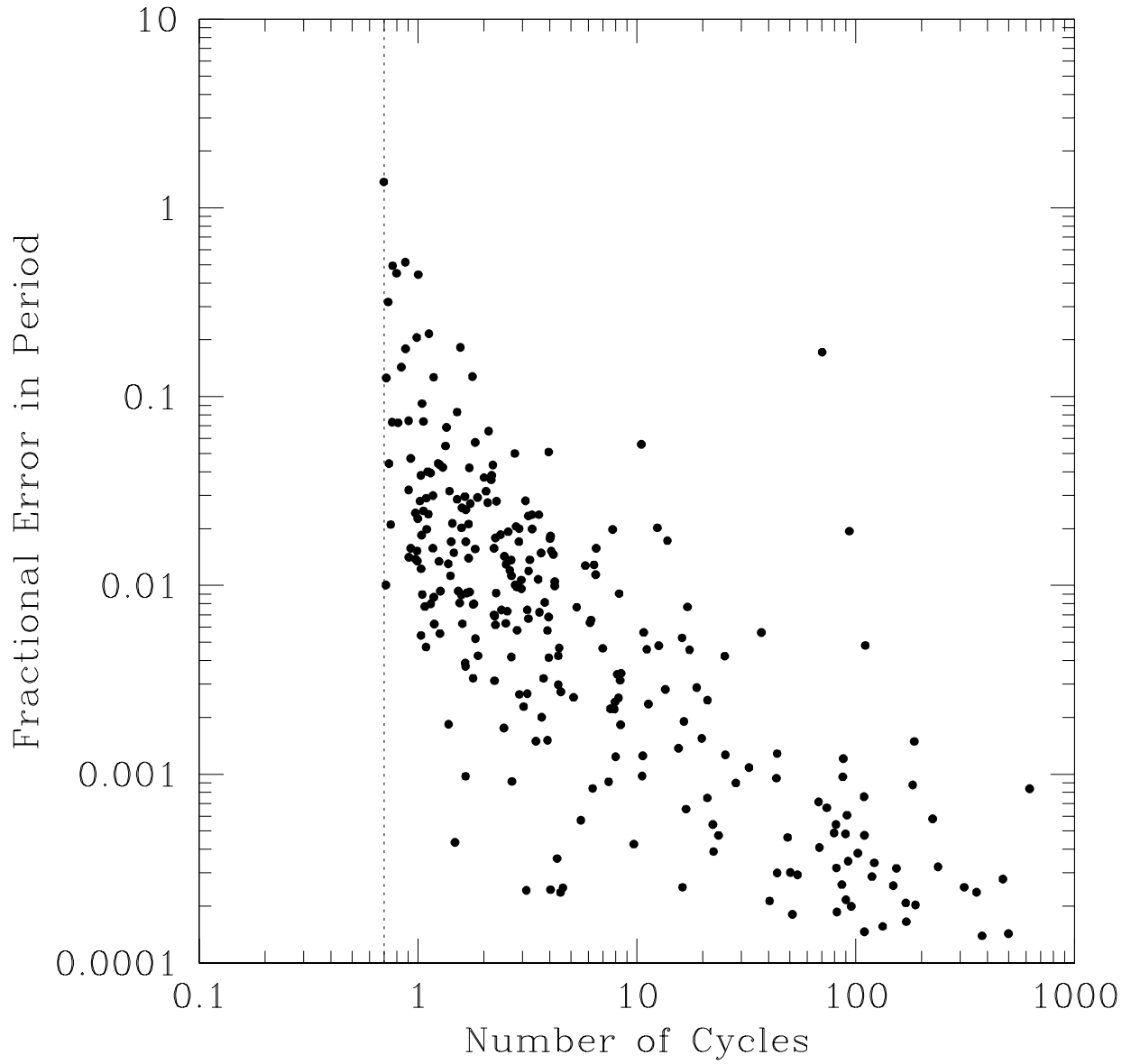


Fig. 4.— Fractional error in orbital period as a function of the number of cycles observed, for 290 published radial-velocity planets. The vertical dashed line indicates 0.7 cycles of data, which appears to be the minimum for publication.

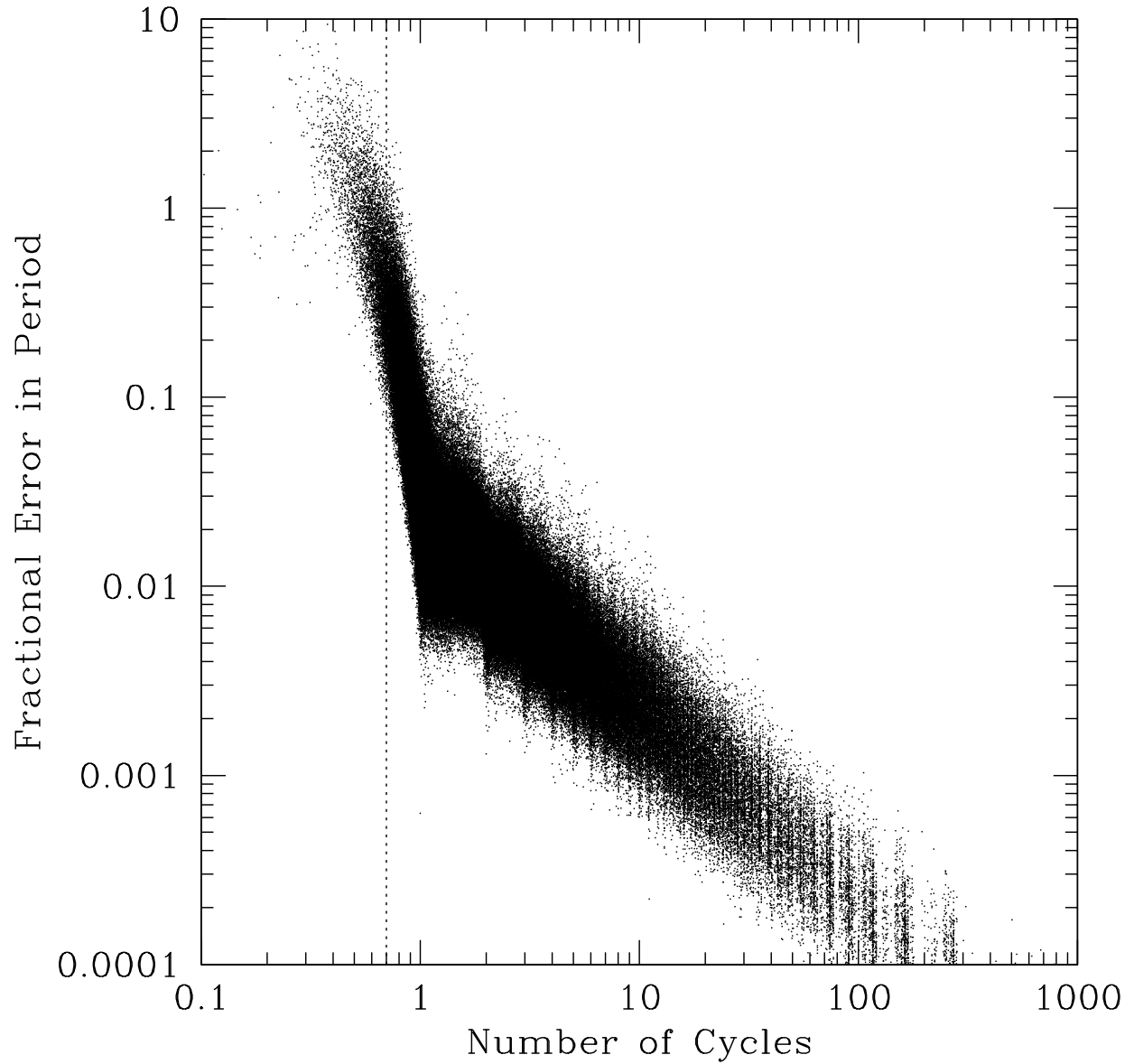


Fig. 5.— Fractional error in orbital period as a function of the number of cycles observed, for 362953 simulated radial-velocity planets. As in Figure 4, the vertical dashed line indicates 0.7 cycles of data. Note that the slope of the relation becomes markedly steeper when less than one cycle is available.

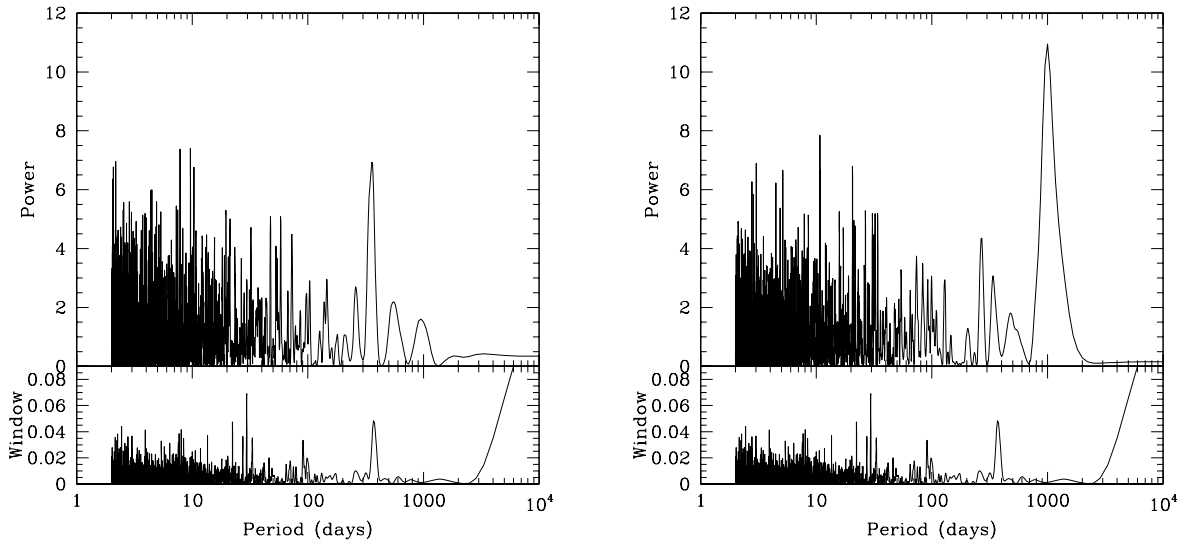


Fig. 6.— An example of a rejected (left panel) and an accepted (right panel) detection using the method and criteria outlined in Section 3. Both periodograms result from the addition of a signal at $P = 1000$ days to the velocity data for HD 209653. The injected signals have $K = 1 \text{ m s}^{-1}$ (left) and 10 m s^{-1} (right).

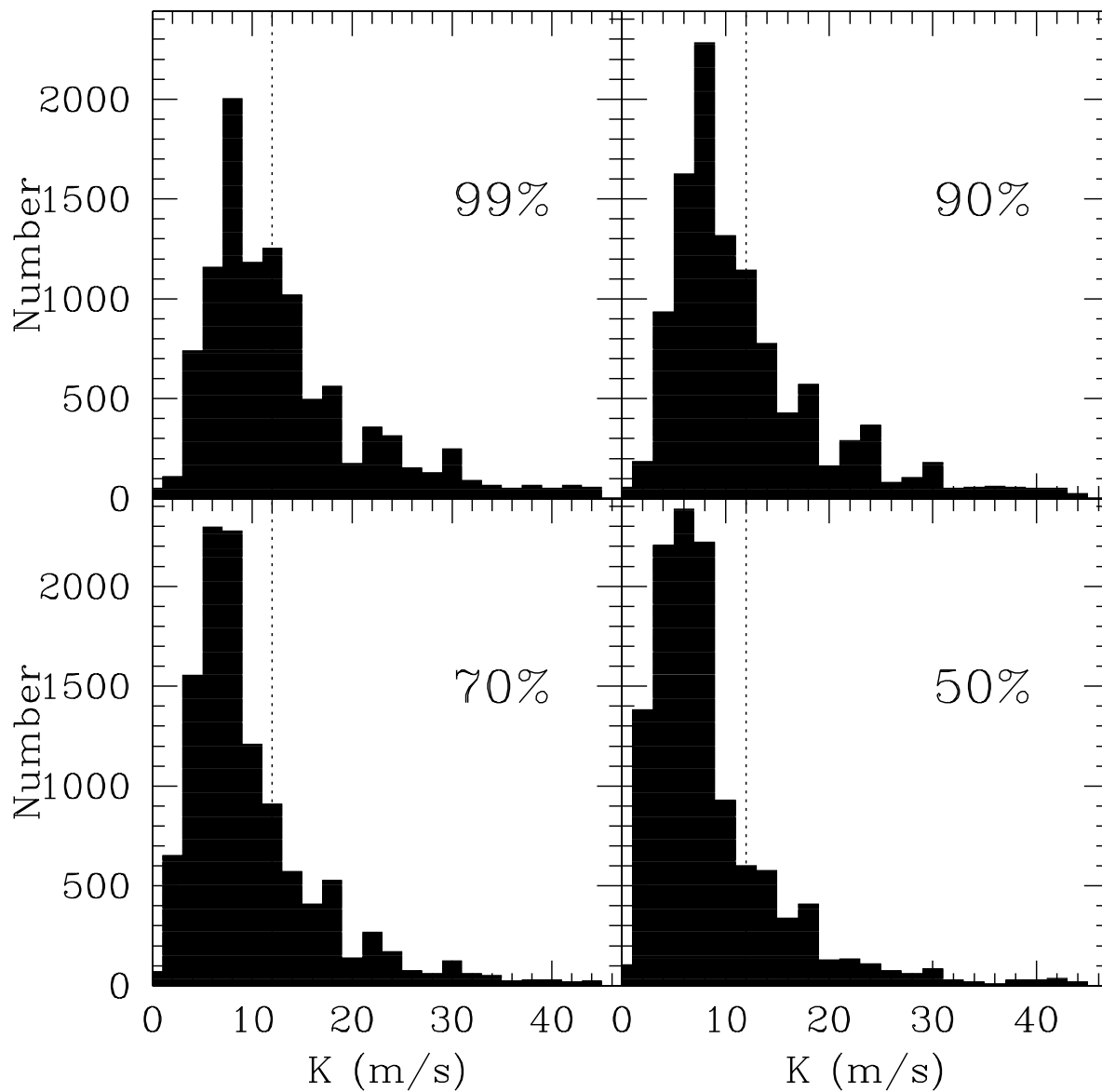


Fig. 7.— Distribution of velocity amplitudes (K) recovered for simulated planets with $e = 0.0$, at recovery levels of 99, 90, 70, and 50%. Each panel shows results from all 123 stars (12300 trial K values). Only $K < 50\text{m s}^{-1}$ is shown; this range includes 91.7% of trials. The vertical dotted line at $K = 12\text{ m s}^{-1}$ indicates the radial-velocity signal of Jupiter.

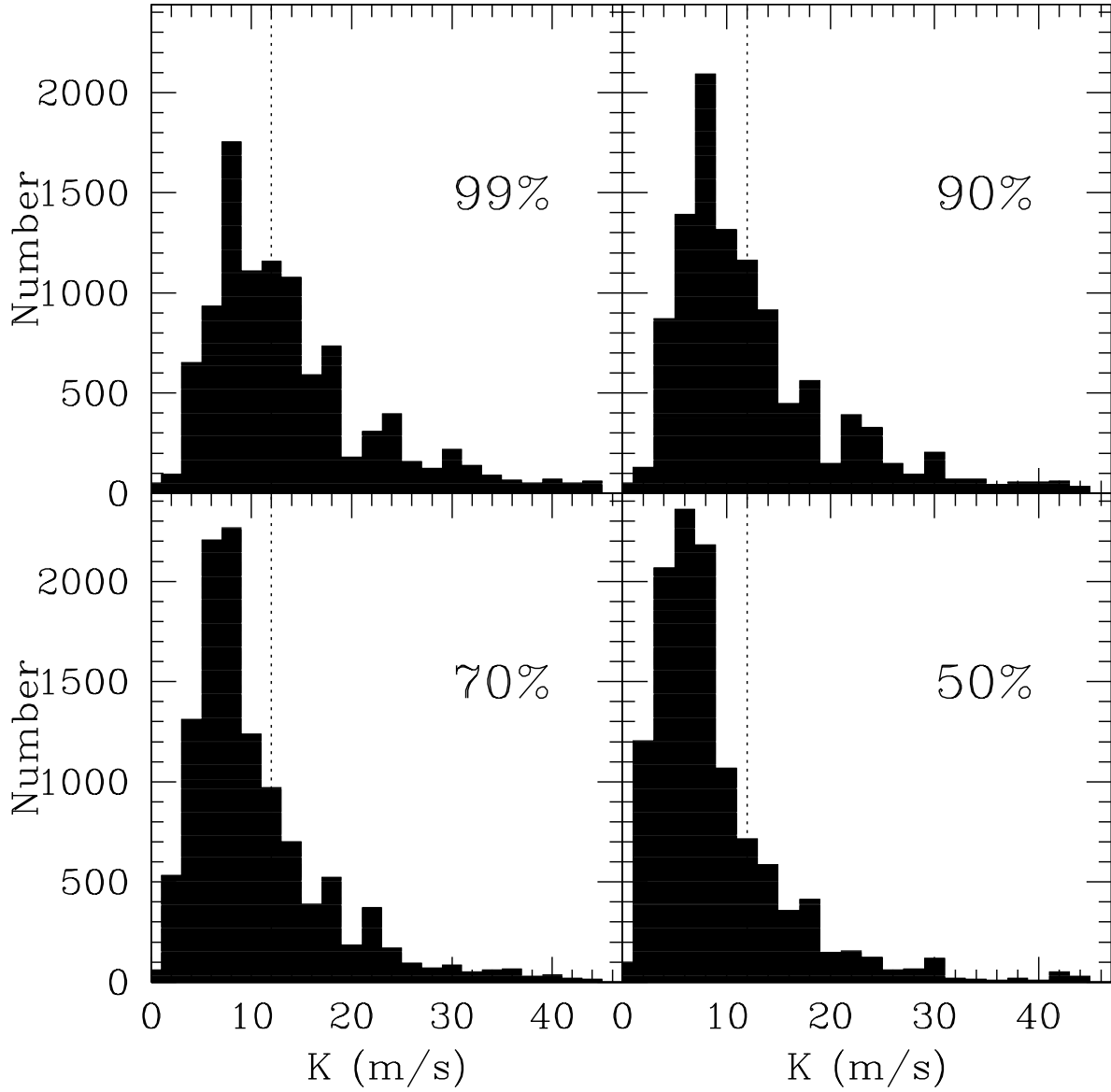


Fig. 8.— Same as Figure 7, but for the $e = 0.1$ results. Only $K < 50 \text{ m s}^{-1}$ is shown; this range includes 90.4% of trials.

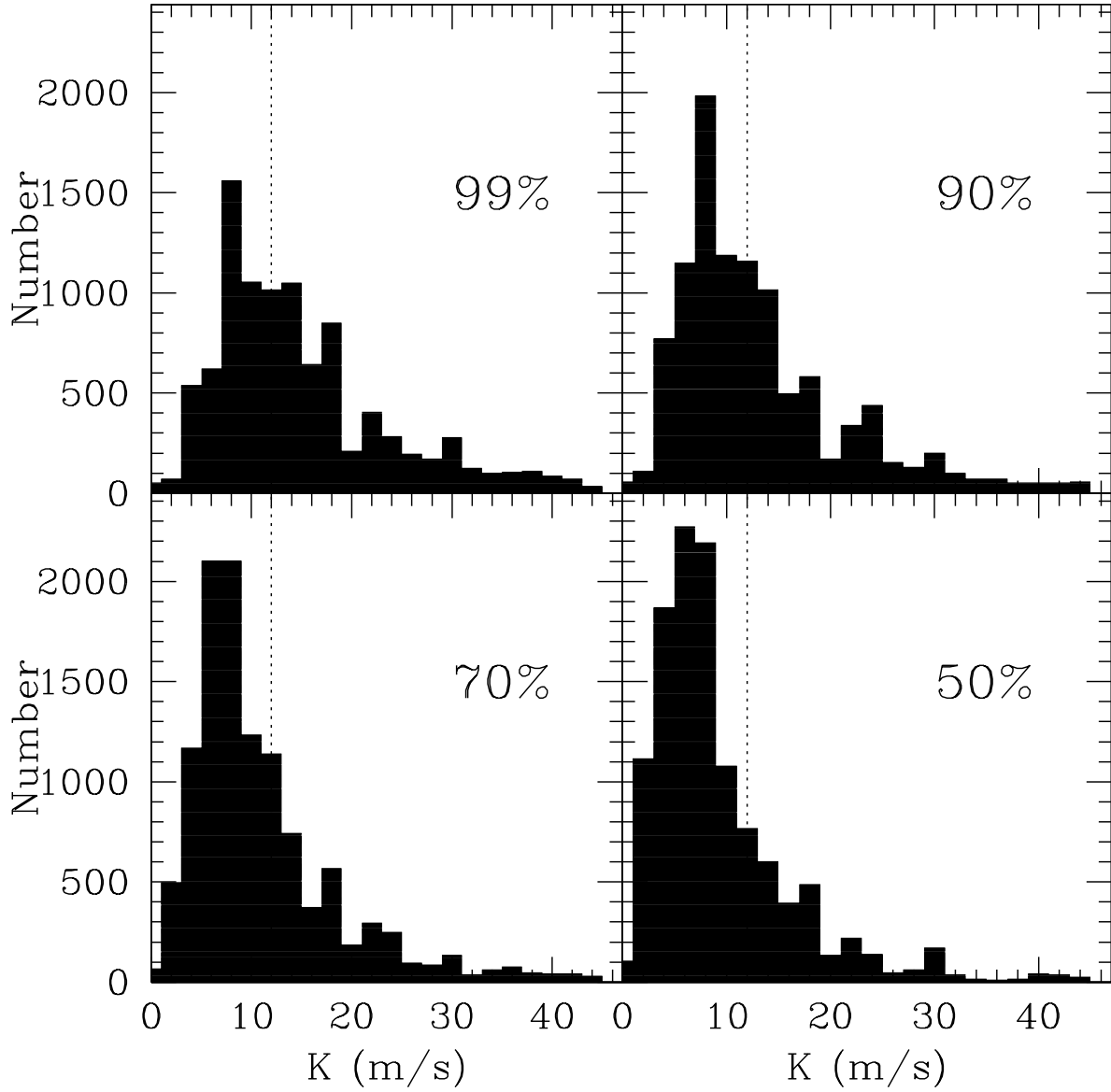


Fig. 9.— Same as Figure 7, but for the $e = 0.2$ results. Only $K < 50 \text{ m s}^{-1}$ is shown; this range includes 88.8% of trials.

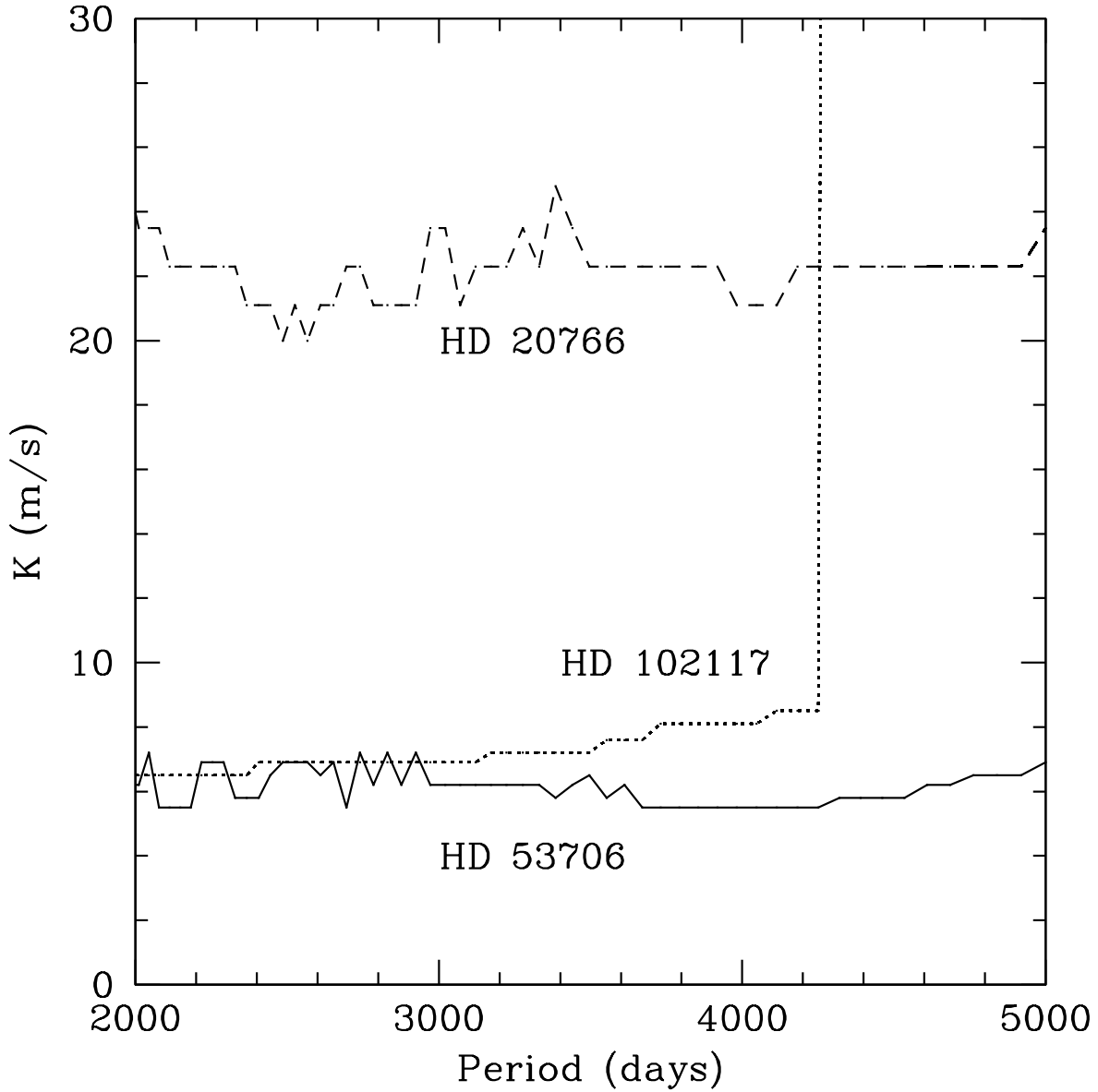


Fig. 10.— Detection limits computed for three representative stars, at 99% recovery. In terms of the velocity amplitude K , the detection limit is essentially constant for a given star, for periods shorter than the duration of observations. At periods longer than the observational data, the injected test signals cannot be robustly detected by our automated criteria, as seen for HD 102117 here ($T_{obs}=3961$ days).

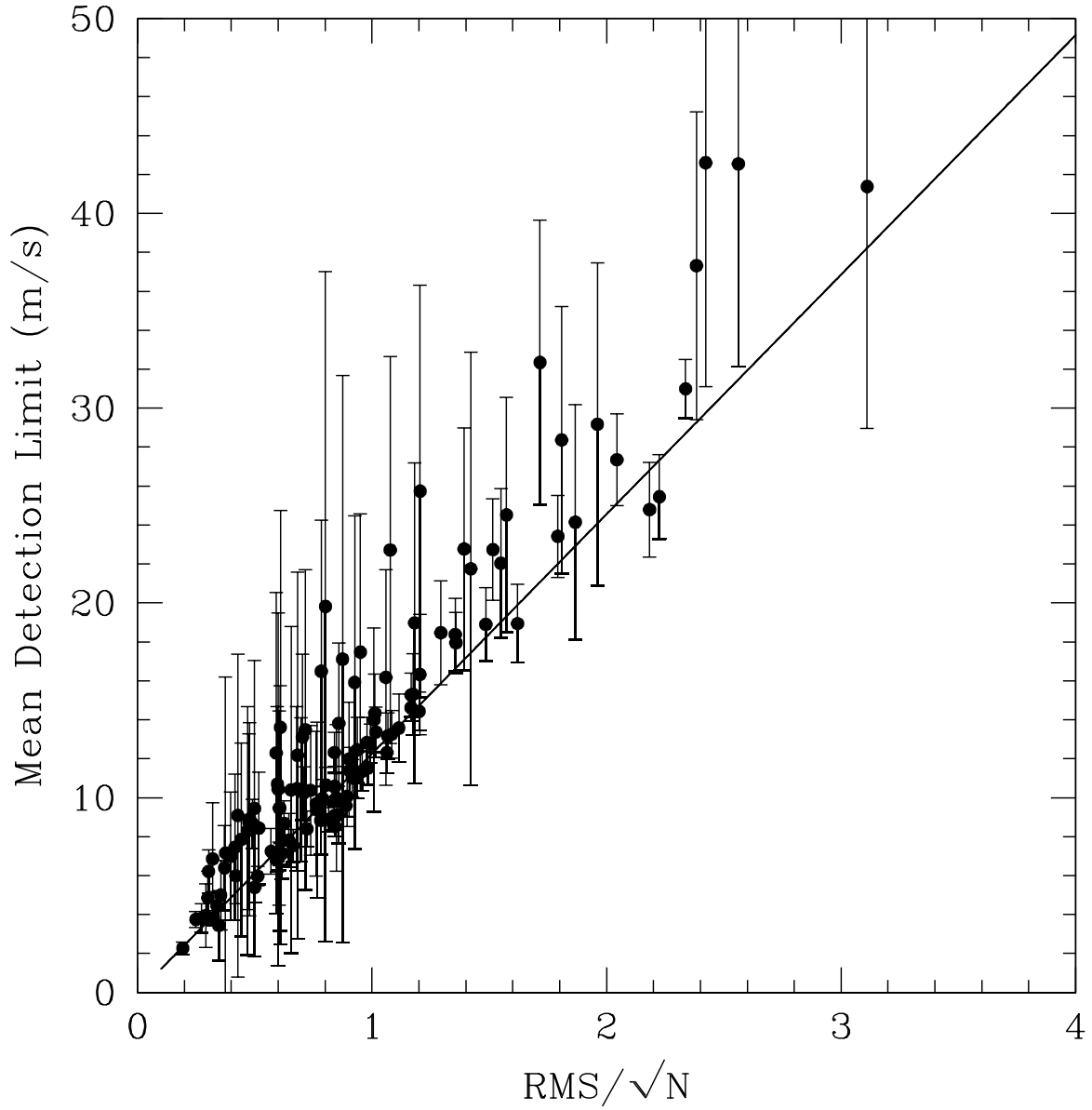


Fig. 11.— Radial-velocity amplitude K that can be detected at the 99% confidence level, plotted against RMS/\sqrt{N} , for 119 stars. A linear relation can be fit, with a scatter of 3.6 m s^{-1} . The solid line is a weighted fit, which is dominated by the abundance of points at $K < 15 \text{ m s}^{-1}$ with small error bars.

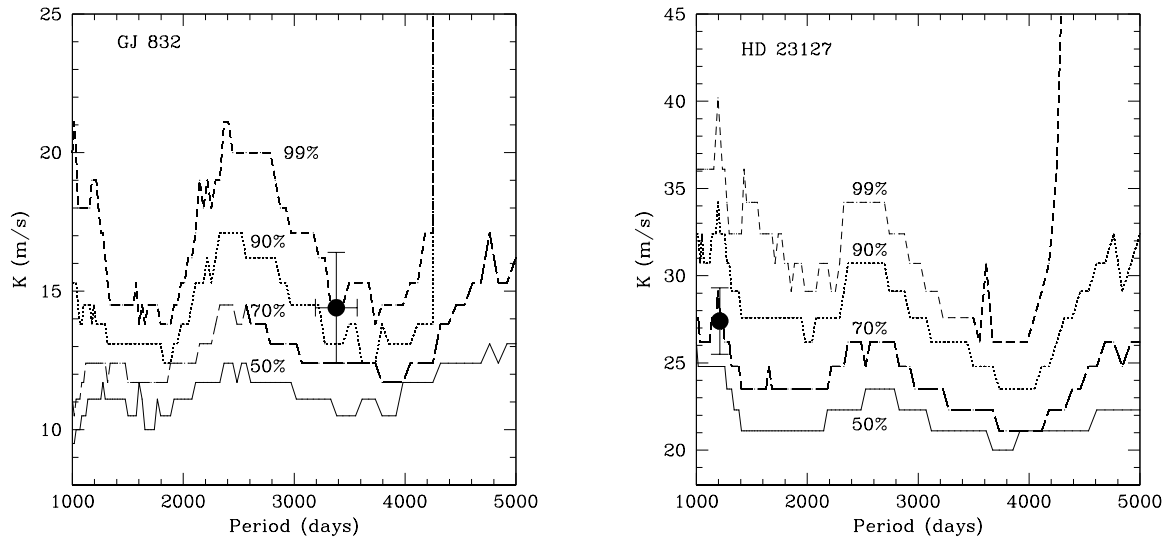


Fig. 12.— Detection limits for GJ 832 (left) and HD 23127 (right) at $e = 0.2$. The known planet is plotted as a large point with error bars. At the specific period of each planet, the detectability is 99% for GJ 832 and 70% for HD 23127. This shows that the automated detection criteria used in this work are more conservative than a human investigator.

Table 3. Substellar Companions From This Sample^a

Planet	Period (days)	T_0 (JD-2400000)	e	ω (degrees)	K (m s^{-1})	M sin i (M_{Jup})	a (AU)	Discovery Ref.
HD 142 b	350.0±3.6	51960±43	0.3±0.18	303±...	34±4.7	1.3±0.32	1.045±0.061	Tinney et al. (2002)
HD 2039 b	1166±11	54405±9	0.574±0.048	344±5	72.1±4.3	3.77±0.45	2.41±0.13	Tinney et al. (2003)
HD 4308 b	15.609±0.007	50108.5±1.9	0.27±0.12	210±21	3.6±0.3	13.0±1.4	0.118±0.009	Udry et al. (2006)
HD 16417 b	17.24±0.01	50099.7±3.3	0.20±0.09	77±26	5.0±0.4	0.067±0.009	0.14±0.01	O’Toole et al. (2009b)
HD 20782 b	585.86±0.03	51687±2.5	0.93±0.03	147±3	120±12	1.8±0.3	0.14±0.01	Jones et al. (2006)
HD 23127 b	1211±16	53649±31	0.396±0.090	183±10	27.4±1.9	1.52±0.13	2.39±0.08	O’Toole et al. (2007)
HD 27442 b	428±1.1	50840±55	0.06±0.04	216±...	32.0±1.4	1.5±0.5	1.27±0.07	Butler et al. (2001)
HD 39091 b	2086±3	50036±3	0.638±0.005	330.6±0.7	194.4±1.2	10.02±0.20	3.31±0.03	Jones et al. (2002)
HD 70642 b	2167±21	51853±177	0.068±0.039	295±29	27.8±1.1	1.82±0.11	3.33±0.05	Carter et al. (2003)
HD 75289 b	3.50927±0.000064	50830.3±0.475	0.03±0.03	141±...	55±1.8	0.46±0.04	0.048±0.003	Udry et al. (2000)
HD 76700 b	3.9710±0.0002	51213.3±0.7	0.10±0.08	30±...	28±1.7	0.23±0.03	0.0511±0.0030	Tinney et al. (2003)
HD 102117 b	20.813±0.006	50942±3	0.12±0.08	279±...	12.0±1.0	0.17±0.02	0.1532±0.0088	Tinney et al. (2005)
HD 117618 b	25.83±0.02	50832±2	0.4±0.17	250±19	13±2.2	0.18±0.05	0.175±0.010	Tinney et al. (2005)
HD 134987 b	258.19±0.07	50071.0±0.8	0.233±0.002	352.7±0.5	49.5±0.2	1.59±0.02	0.81±0.02	Jones et al. (2010)
HD 160691 b	643.25±0.90	52366±13	0.13±0.017	22±7	37.8±0.4	1.7±0.13	1.497±...	Butler et al. (2001)
HD 160691 d	9.6386±0.0015	52991.1±0.4	0.17±0.04	210±13	3.1±0.13	0.035±0.003	0.0909±...	Santos et al. (2004)
HD 160691 e	310.55±0.83	52708.7±8.3	0.07±0.01	189.6±9.4	14.9±0.6	0.54±0.04	0.921±...	Pepe et al. (2007)
HD 164427 b	108.55±0.04	51724.6±0.2	0.55±0.02	356.9±0.5	2229±77	46.4±3.4	0.46±0.05	Tinney et al. (2001)
HD 179949 b	3.09251±0.00003	51002.4±0.4	0.02±0.015	192±...	113±1.8	0.90±0.07	0.0443±0.0026	Tinney et al. (2001)
HD 187085 b	1065±19	51392±325	0.047±0.090	261±114	15.3±1.4	0.88±0.13	2.19±0.08	Jones et al. (2006)
HD 196050 b	1398±15	54973±55	0.181±0.030	174±11	49.4±1.4	3.02±0.22	2.60±0.07	Jones et al. (2002)
HD 208487 b	130.1±0.51	51000±16	0.2±0.16	113±...	20±3.6	0.5±0.13	0.524±0.030	Tinney et al. (2005)
HD 213240 b	883±7.6	51500±13	0.42±0.02	201±3	97±2	4.5±0.34	1.92±0.11	Santos et al. (2001)
HD 216435 b	1339±16	50632±158	0.069±0.062	41±42	19.8±1.1	1.28±0.12	2.60±0.06	Jones et al. (2003)
HD 216437 b	1355±7	51942±18	0.357±0.025	61±5	39.0±1.1	2.22±0.08	2.54±0.03	Jones et al. (2002)
Jupiter analogs								
HD 134987 c	5000±400	51100±600	0.12±0.02	195±48	9.3±0.3	0.82±0.03	5.8±0.5	Jones et al. (2010)
HD 160691 c	4163±99	52513±62	0.029±0.024	23±48	23.2±0.5	2.00±0.10	5.3±0.1	McCarthy et al. (2004)
GJ 832 b	3380±189	54618±374	0.157±0.015	305±40	14.4±2.0	0.62±0.13	3.38±0.40	Bailey et al. (2009)

^aThose 123 stars with $N > 30$ and $T_{obs} > 8$ yr.

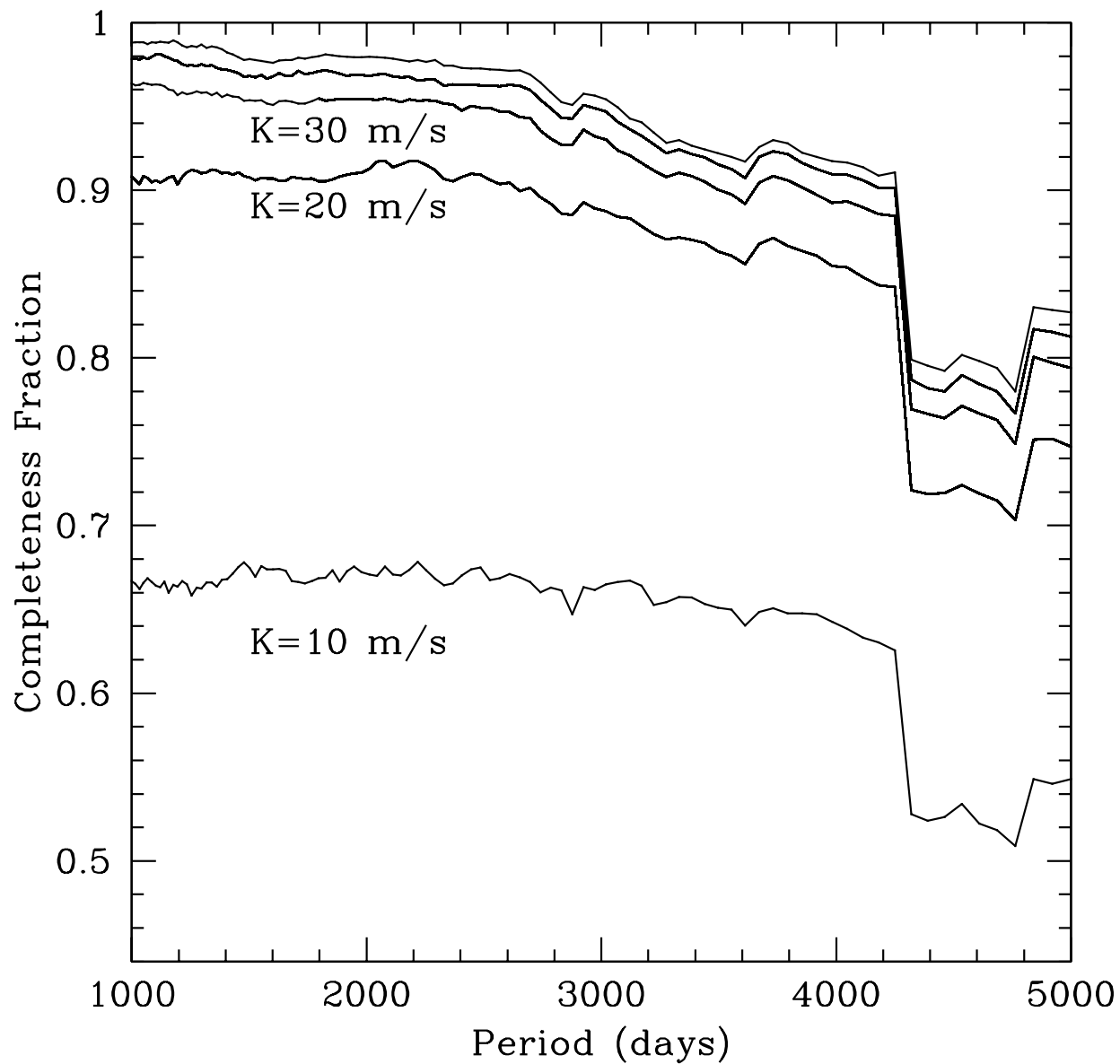


Fig. 13.— Completeness fraction $f_c(P_i, K_i)$ (Equation 2) summed over 101 AAPS stars, as a function of orbital period and radial-velocity amplitude K . From bottom to top, the curves are for $K = 10, 20, 30, 40,$ and 50 m s^{-1} . The drop-off in completeness at $P \sim 4300$ days occurs because that is the maximum duration of observations for any star in the sample.

Table 4. Jupiter-Analog Upper Limits from the AAPS Sample

Velocity Amplitude (m s^{-1})	Upper Limit percent		
	e=0.0	e=0.1	e=0.2
$K > 50$	11.6 ± 1.1	12.3 ± 1.4	14.6 ± 1.5
$K > 40$	12.6 ± 1.1	13.6 ± 1.4	16.2 ± 1.5
$K > 30$	14.4 ± 1.2	15.4 ± 1.4	18.6 ± 1.5
$K > 20$	18.6 ± 1.1	20.7 ± 1.5	23.8 ± 1.6
$K > 10$	37.2 ± 1.1	44.8 ± 1.4	48.8 ± 1.5